


---

This is the **accepted version** of the journal article:

Puigcorbé, Viena [et al.]. «Particulate organic carbon export across the Antarctic Circumpolar Current at 10°E : Differences between north and south of the Antarctic Polar Front». *Deep-Sea Research Part II: Topical Studies in Oceanography*, Vol. 138 (April 2017), p. 86-101 DOI 10.1016/j.dsr2.2016.05.016

---

This version is available at <https://ddd.uab.cat/record/323466>

under the terms of the  license.

**Particulate organic carbon export across the Antarctic Circumpolar Current at 10°E:  
Differences north and south of the Antarctic Polar Front**

V. Puigcorbé<sup>1,2</sup>, M. Roca-Martí<sup>1</sup>, P. Masqué<sup>1,2,3</sup>, C.R. Benitez-Nelson<sup>4</sup>, M. Rutgers  
v. d. Loeff<sup>5</sup>, L.M. Laglera<sup>6</sup>, A. Bracher<sup>5,7</sup>, W. Cheah<sup>5,8</sup>, V. Strass<sup>5</sup>, M. Hoppema<sup>5</sup>, J.  
Santos-Echeandía<sup>9</sup>, B.P.V. Hunt<sup>10,11</sup>, E.A. Pakhomov<sup>10</sup>, C. Klaas<sup>5</sup>

<sup>1</sup>Institut de Ciència i Tecnologia Ambientals & Departament de Física, Universitat Autònoma de  
Barcelona, 08193 Bellaterra, Spain

<sup>2</sup>School of Natural Sciences and Centre for Marine Ecosystems Research, Edith Cowan  
University, Joondalup WA 6027, Australia

<sup>3</sup>Oceans Institute and School of Physics, The University of Western Australia, Crawley WA 6009,  
Australia

<sup>4</sup>Marine Science Program & Department of Earth & Ocean Sciences, University of South  
Carolina, Columbia, SC 29208, USA

<sup>5</sup>Alfred Wegener Institute, Helmholtz Centre for Polar and Marine Research, 27570 Bremerhaven,  
Germany

<sup>6</sup>FI-TRACE, Departament de Química. Universitat de les Illes Balears, Palma, E-07122 Spain

<sup>7</sup>Institute of Environmental Physics, University of Bremen, 28359 Bremen, Germany

<sup>8</sup>Research Center for Environmental Changes, Academia Sinica, 11529 Taipei, Taiwan

<sup>9</sup>Grupo de Biogeoquímica Marina, Instituto de Investigaciones Marinas (CSIC) Eduardo Cabello,  
Vigo, E-36208, Spain

<sup>10</sup>Department of Earth, Ocean and Atmospheric Sciences, University of British Columbia,  
V6T1Z4 Vancouver, Canada

<sup>11</sup>Hakai Institute, P.O. Box 309, Heriot Bay, BC, V0P 1H0, Canada

## 28    **ABSTRACT**

29    The vertical distribution of  $^{234}\text{Th}$  was measured along the 10°E meridian between 44°S and 53°S in  
30    the Antarctic Circumpolar Current (ACC) during the austral summer of 2012. The overarching  
31    goal of this work was to estimate particulate organic carbon (POC) export across three fronts: The  
32    Sub-Antarctic Front (SAF), the Antarctic Polar Front (APF) and the Southern Polar Front (SPF).  
33    Steady state export fluxes of  $^{234}\text{Th}$  in the upper 100 m ranged from 1600 to 2600  $\text{dpm m}^{-2} \text{d}^{-1}$ ,  
34    decreasing with increasing latitude. Using large particle ( $>53 \mu\text{m}$ )  $\text{C}/^{234}\text{Th}$  ratios, the  $^{234}\text{Th}$ -derived  
35    POC fluxes at 100 m ranged from 25 to 41  $\text{mmol C m}^{-2} \text{d}^{-1}$ . Observed  $\text{C}/^{234}\text{Th}$  ratios decreased  
36    with increasing depth north of the APF, while south of the APF, ratios remained similar or even  
37    increased with depth. These changes in  $\text{C}/^{234}\text{Th}$  ratios are likely due to differences in the food  
38    web. Indeed, satellite images, together with macronutrients and dissolved iron concentrations  
39    suggest two different planktonic community structures north and south of the APF. Our results  
40    indicate that higher ratios of POC flux at 100 m to primary production occurred in  
41    nanophytoplankton dominated surface waters, where primary production rates were lower.  
42    Satellite images prior to the expedition suggest that the higher export efficiencies obtained in the  
43    northern half of the transect may be the result of the decoupling between production and export  
44    (Buesseler 1998). Transfer efficiencies to 400 m, i.e. the fraction of exported POC that reached  
45    400 m, were found to be higher in the south of the APF, where diatoms were dominant and salps  
46    largely abundant. This suggests different remineralization pathways of sinking particles,  
47    influencing the transfer efficiency of exported POC to depth.

## 48 1. INTRODUCTION

49 The Southern Ocean (SO) is a key component of Earth's climate through its pivotal role in the  
50 regulation of atmospheric carbon dioxide (CO<sub>2</sub>) and nutrient supply to other ocean basins (Gruber  
51 et al., 2009; Landschützer et al., 2015; Sarmiento et al., 2004; Takahashi et al., 2009). The SO  
52 consists of several hydrographic and biogeochemical regions delimited by zonal fronts, mostly  
53 characterized by strong horizontal temperature and salinity gradients (Orsi et al., 1995; Pollard et  
54 al., 2002b; Whitworth and Nowlin, 1987). The region between the southern limit of the Antarctic  
55 Polar Front (APF) and the southern boundary of the Antarctic Circumpolar Current (ACC) is  
56 characterized by upwelling of nutrient- and CO<sub>2</sub>-rich deep waters (Hoppema et al., 2000; Nowlin  
57 and Klinck, 1986; Tomczak and Godfrey, 2001) and as a consequence, high macronutrients  
58 concentrations occur in the surface waters with persistent high concentrations of unused nitrate in  
59 a sufficiently lit and stratified euphotic zone.

60 Several *in situ* artificial iron fertilization experiments have shown that the low phytoplankton  
61 concentrations and productivity within the SO are due to iron limitation (Boyd et al., 2007; Coale  
62 et al., 2004; Smetacek et al., 2012). Changes in SO iron input and the resulting increase in  
63 particulate carbon export to greater depths (through the "biological pump") are hypothesized to be  
64 responsible for an approximately 30 ppm decrease in atmospheric CO<sub>2</sub> during glacial periods  
65 (Aumont and Bopp, 2006; Köhler et al., 2005). A better understanding of the relationship between  
66 primary productivity and the efficiency of the biological carbon pump is thus required in order to  
67 determine past and present climate change impacts on the SO carbon cycle and atmospheric CO<sub>2</sub>.  
68 Previous studies have shown that export of organic matter to the deep ocean is not necessarily  
69 proportional to primary production rates (e.g., Buesseler, 1998), and discrepancies exist between  
70 models and *in situ* measurements (Arrigo et al., 1998; Gruber et al., 2009; Maiti et al., 2013).  
71 Sediment traps have shown regional variations among the various circumpolar zones and zonal  
72 sectors in particulate organic carbon (POC) export to the deep sea (see Boyd and Trull, 2007 and

73 references therein). However, scarce spatial coverage of sediment traps studies, and the possible  
74 biases associated with traps (mainly due to hydrodynamics and solubilization; Buesseler et al.,  
75 2007; Usbeck et al., 2003) warrant the use of other complementary approaches to quantify the  
76 spatial and temporal variability of the biological pump in the SO.

77 A widely applied approach to estimate particle export is the use of the radionuclide pair  
78  $^{234}\text{Th}/^{238}\text{U}$ . Thorium-234 is a naturally occurring, short-lived radionuclide ( $T_{1/2} = 24.1$  days)  
79 produced by the alpha decay of  $^{238}\text{U}$  ( $T_{1/2} = 4.5 \times 10^9$  years). Due to its high particle affinity,  
80 thorium is rapidly adsorbed onto particle surfaces (Moore and Millward, 1988). In contrast  
81 uranium is conservative in oxic systems (Chen et al., 1986). Thus, the deviation of  $^{234}\text{Th}/^{238}\text{U}$  from  
82 unity can be used as a proxy for particle dynamics (e.g., formation and export) in the ocean  
83 surface. Further, the half-life of  $^{234}\text{Th}$  is similar to the time scales of processes that determine  
84 particle dynamics in the ocean (such as the development of phytoplankton blooms), allowing for  
85 fine-scale observations of particle export and remineralization.

86 The fronts of the ACC have been found to coincide with boundaries between regions of similar  
87 phytoplankton biomass (Sokolov and Rintoul, 2007). Moreover, phytoplankton composition and  
88 distribution appear to be strongly linked to physical zonation within the SO (Laubscher et al.,  
89 1993; Read et al., 2002). Sediment records also reflect such boundaries, with large opal  
90 accumulation found south of the APF (Geibert et al., 2005; Tréguer and De La Rocha, 2013), as a  
91 consequence of spatial segregation of phytoplankton communities due to difference temperature  
92 and nutrient regimes (Falkowski et al., 1998). This in turn also affects zooplankton community  
93 composition and distribution (Hunt and Hosie, 2005; Pakhomov and McQuaid, 1996; Pollard et  
94 al., 2002a) and their grazing dynamics. Thus, physical controls on biogeochemical zonation are  
95 expected to influence the pelagic community structure, which will affect the composition of the  
96 sinking particles, and hence the downward flux of organic matter (Korb et al., 2012; Quéguiner,  
97 2013)

98 In this study, we present new estimates of late summer POC export flux for the Atlantic sector of  
99 the SO, along the 10°E meridian, across four different frontal zones: the Sub-Antarctic zone  
100 (SAZ), the Polar Frontal Zone (PFZ), the Antarctic Zone (AZ), and the Southern Zone (SZ). Our  
101 aim is to assess how the physical boundaries and zonal biology affect the magnitude and the  
102 efficiency of surface POC export and its transfer efficiency to depth. To do so, we analyzed water  
103 column distributions of  $^{234}\text{Th}$ , combined with the measured ratio of POC/ $^{234}\text{Th}$  (hereafter C/ $^{234}\text{Th}$ )  
104 in order to obtain POC export fluxes and examine their variability as a function of physical  
105 oceanographic conditions, primary productivity and planktonic community stocks and  
106 composition.

## 107 2. MATERIALS AND METHODS

108 Samples were collected along a meridional transect at 10°E, between 44°S to 53°S, from the 11<sup>th</sup> to  
109 the 22<sup>nd</sup> of January, 2012 (Figure 1) within the framework of the Eddy-Pump survey during the  
110 R/V *Polarstern* cruise ANT-XXVIII/3 (Wolf-Gladrow, 2013).

### 111 2.1 *Th-234*

112 Six stations (St. 57, 63, 69, 75, 81 and 84) were sampled for total  $^{234}\text{Th}$  using a CTD-rosette  
113 equipped with 12 L Niskin bottles (Figure 1f; Table 1). Seawater samples (4 L each) were  
114 collected at 12 discrete depths in the upper 500 m of the water column, acidified to pH <2 with  
115 nitric acid and spiked with a known amount of  $^{230}\text{Th}$ . Samples were processed using the  $\text{MnO}_2$  co-  
116 precipitation technique (Benitez-Nelson et al., 2001) and counted on board using a gas flow  
117 proportional low-level background beta counter (counting statistics <3%) (RISØ, Denmark).  
118 Samples were recounted after 5-7 months to determine background activities.

119  $\text{Th-230}$  recoveries were measured with an adaptation of the method described in Pike et al. (2005),  
120 where the column purification step was removed. Briefly, the  $\text{MnO}_2$  precipitate was dissolved in  
121 10 ml of 8M  $\text{HNO}_3$ /10%  $\text{H}_2\text{O}_2$  solution and a known amount of  $^{229}\text{Th}$  was added as a second yield

122 tracer. Samples were sonicated for 30 min and allowed to stand covered for 6 h. Once the filter  
123 was dissolved, the remaining solution was evaporated to dryness and reconstructed to 5% HNO<sub>3</sub>  
124 and 0.08% HF and then filtered using Acrodisc 0.2 µm HT Tuffryn membrane syringe filters  
125 (Whatman). An aliquot was then taken from the filtered solution and diluted with 2.2% HNO<sub>3</sub>  
126 before measuring the <sup>230</sup>Th/<sup>229</sup>Th using ICP-MS. Average recoveries of 95 ± 5% were obtained (n  
127 = 68). <sup>238</sup>U activities (in units of dpm L<sup>-1</sup>) were determined from salinity data using the  
128 relationship from Owens et al. (2011) where <sup>238</sup>U (± 0.047) = (0.0786 ± 0.00446) × S – (0.315 ±  
129 0.158). Calibration for the relative efficiency of the detectors was carried out using <sup>238</sup>U standards.  
130 Replicate deep water samples (2500 m) were collected at selected stations to confirm the  
131 calibration, with a resulting <sup>234</sup>Th/<sup>238</sup>U activity ratio of 1.05 ± 0.09 (n = 7), consistent with that  
132 expected for secular equilibrium. Uncertainties for the <sup>234</sup>Th activity were calculated by  
133 propagating errors associated with counting, calibration, background corrections and <sup>238</sup>U  
134 activities and were always <10%. The laboratories where samples were processed and analyzed  
135 participated in the intercomparison of <sup>234</sup>Th measurements in both water and particulate samples,  
136 as part of the GEOTRACES inter-calibration program (Maiti et al., 2012).

## 137 **2.2 Particulate samples**

138 Samples for analysis of particulate matter composition and particle associated <sup>234</sup>Th were collected  
139 at 100 and 300 or 400 m depth using *in situ* pumps (ISP; *Challenger Oceanic*) equipped with 142  
140 mm diameter filter holders. Samples were taken at the same stations as seawater <sup>234</sup>Th profiles,  
141 except those at 46°S and 50°S. Between 840 and 1500 L seawater was filtered through 53 µm  
142 pore-size Nitex screens. The particulate material was rinsed from the screen using filtered  
143 seawater, collected in an acid-cleaned plastic beaker and stirred to homogenize the sample. A  
144 volumetric fraction of the rinse solution, representing ~30% of the total volume, was filtered onto  
145 pre-combusted 25 mm quartz filters (QMA, Millipore) for <sup>234</sup>Th analysis. Another aliquot of a  
146 similar volume was also filtered through a pre-combusted QMA filter for POC and particulate

147 organic nitrogen (PON) analyses (see section 2.5). Filters were dried overnight at 50°C. <sup>234</sup>Th  
148 particulate samples were counted at sea and recounted for background activities 5-7 months later,  
149 as was done for the water samples, with associated uncertainties <10%.

### 150 **2.3 Dissolved Fe**

151 Five stations (St. 60, 70, 76, 81 and 84) were sampled for dissolved iron profiles (DFe) using  
152 metal-free GO-FLO bottles attached to a Kevlar line, at 5 to 7 discrete depths between 20 and 300  
153 m. The GO-FLO bottles were transferred to a clean plastic “bubble” where the atmosphere was  
154 kept clean by over pressurization with filtered air. DFe samples (~ 60 mL) were collected in 60  
155 mL LDPE bottles directly from the GO-FLO bottles using pressurized nitrogen and inline 0.2 µm  
156 pore size sterile capsules (Sartobran 300).

157 Seawater DFe concentrations were determined onboard according to the voltammetric method  
158 which is based on the electroactivity of iron complexed to DHN (Laglera et al., 2013). Briefly,  
159 immediately after filtration, samples were spiked with 12 µL HCl (30%; Merk, Trace Select) per  
160 10 mL seawater for a pH of 2.0 (NBS scale) and 30 µM of DHN (2,3-dihydroxynaphthalene).  
161 After allowing equilibration for 24 h at room temperature, samples were spiked with 500 µL of a  
162 BrO<sub>3</sub><sup>-</sup>/POPSO solution, and adjusted to pH ~8.7 with NH<sub>4</sub>OH (15%, UltraTrace, Sigma).  
163 Analytical sensitivity was determined for each sample using two standard additions of 0.3 nM  
164 iron. The settings of the voltammetric analysis and other additional information can be found in  
165 Laglera et al. (2013).

### 166 **2.4 Nutrients and dissolved oxygen**

167 Macronutrients were analyzed colorimetrically on board using a Technicon TRAACS 800 auto-  
168 analyzer (Seal Analytical), according to Grasshoff et al. (1983) (for nitrate), Murphy and Riley  
169 (1962) (for phosphate) and Strickland and Parsons (1968) (for silicate). Details regarding the  
170 complete procedure are given in Hoppe et al. (this issue).



171 Vertical profiles of dissolved oxygen through the entire water column (at about 20 discrete depths)  
172 were determined at all stations along the section. Oxygen concentrations were measured using a  
173 standard automated Winkler technique with photometric endpoint detection. The precision as  
174 determined by the mean difference of duplicates was 0.7  $\mu\text{mol/kg}$ , or better than 0.3% coefficient  
175 of variation.

## 176 **2.5 POC and PON**

177 POC and PON concentrations in the upper water column were measured on 1 to 2 L seawater  
178 samples collected directly from the Niskin bottles attached to the CTD-rosette at 7-8 discrete  
179 depths (between 10 and 200 m depth). Samples were filtered onto pre-combusted 25 mm diameter  
180 GFF filters and stored in pre-combusted glass petri dishes. After filtration, filters were dried  
181 overnight at 50°C and stored at -20°C for further analysis on land. Before analysis, samples were  
182 thawed at room temperature and a few drops of 0.1 M HCl were added to the filters to dissolve the  
183 particulate inorganic carbon. Filters were then dried overnight at 50°C. POC and PON  
184 concentrations on the  $^{234}\text{Th}$  filters were also analyzed after beta counting for comparison with  
185 filters from the ISP measured directly for POC and PON, thus comparing two aliquots of the >53  
186  $\mu\text{m}$  size fraction, in order to assess within station variability. All POC and PON measurements  
187 were measured with an EuroVector Elemental Analyzer (Euroanalysator EA). Samples were  
188 corrected for C and N blanks ( $1.37 \pm 0.03 \mu\text{mol C}$  and  $0.20 \pm 0.02 \mu\text{mol N}$ , respectively), and  
189 averaged <10% of each signal. Measurement variability based on reference standard  
190 measurements was 3.6% (N) and 1.9% (C) for the upper water column samples.

## 191 **2.6 Chlorophyll a**

### 192 **2.6.1 Satellite data**

193 In order to capture regional synoptic variability in surface biological processes, merged  
194 chlorophyll-a (Chl-a) data (ESACCI-OC-L3S product, ~4 km, version 2.0,

195 <http://www.oceancolour.org> from the daily Ocean Colour Climate Change Initiative OC-CCI,  
196 2015) was averaged over the time period of interest. The OC-CCI data product provides high  
197 quality ocean color products combining the Medium Resolution Imaging Spectrometer (MERIS)  
198 on Envisat, the Moderate resolution Imaging Spectrometer (MODIS) on the Aqua satellite and the  
199 Sea-viewing Wide Field-of-view Sensor (SeaWiFS) on Orb-View-2 sensors. For the time frame of  
200 this study only MERIS and MODIS data were available. Current data processing improves  
201 limitations of ocean color remote sensing in polar regions due to low solar elevation and frequent  
202 cloud cover. This is achieved by an improved atmospheric correction applied to MERIS data with  
203 the Polymer algorithm (Steinmetz et al., 2011), and to MODIS data following the algorithm of  
204 Gordon and Wang (1994) with several subsequent modifications and improvements according to  
205 IOCCG (2010).

#### 206 2.6.2 *In situ* Chl-*a*

207 Water samples for Chl-*a* determination by means of fluorometry (Chl-*a*<sub>FLUO</sub>) were collected at 8  
208 depths between 10 and 200 m. Samples were filtered onto 25 mm GFF filters and treated  
209 following the method described in Hoppe et al. (this issue). Chl-*a* content was measured in a  
210 Turner 10-AU fluorometer. Calibration of the fluorometer was carried out at the beginning and at  
211 the end of the cruise, with results diverging by 2%. Chl-*a* content was calculated using the  
212 equation given in Knap et al. (1996) using average parameter values from the two calibrations.

213 Chl-*a* concentrations were also determined by high performance liquid chromatography (HPLC;  
214 Chl-*a*<sub>HPLC</sub>). Water samples were filtered and shock-frozen in liquid nitrogen and stored at -80°C  
215 until analysis in the home laboratory following the method of Barlow et al. (1997), as described in  
216 detail in Cheah et al. (this issue). Chl-*a*<sub>HPLC</sub> was calculated as the sum of concentrations of  
217 monovinyl *a* and chlorophyllide *a* (divinyl chlorophyll *a* was below detection in all samples). Chl-  
218 *a* inventories were determined to a depth of 100 m according to the method described by Morel  
219 and Maritorena (2001).

220 As shown by Hoppe et al. (this issue), both Chl-a data sets (Chl-a<sub>HPLC</sub> and Chl-a<sub>FLUO</sub>) were very  
221 similar ( $r^2 = 0.97$ ,  $p < 0.001$ ,  $n = 104$ ,  $\text{Chl-a}_{\text{FLUO}} = 0.990 * \text{Chl-a}_{\text{HPLC}} + 0.0837$ ). Chl-a<sub>HPLC</sub> data was  
222 used to derive primary production rates (see section 3.6).

## 223 ***2.7 Phytoplankton size class analyses***

224 Three pigment-based phytoplankton size classes (micro-, nano-, and picophytoplankton) were  
225 estimated following the procedure as in Uitz et al. (2009), using defined marker pigment  
226 concentrations in relation to Chl-a<sub>HPLC</sub>, which has been tested for the SO waters (e.g., Uitz et al.,  
227 2009). Microphytoplankton corresponds to phytoplankton with size  $>20 \mu\text{m}$ , nanophytoplankton  
228 between  $2\text{--}20 \mu\text{m}$ , and picophytoplankton between  $0.2\text{--}2 \mu\text{m}$ . Detailed description of the  
229 calculation is presented in Cheah et al. (this issue).

## 230 ***2.8 Zooplankton***

231 Zooplankton samples were collected from the upper 250 m of the water column during double  
232 oblique tows using a Rectangular Midwater Trawl (RMT 1+8) equipped with  $1 \text{ m}^2$  (0.33 mm mesh  
233 size) and  $8 \text{ m}^2$  (4.5 mm mesh size) nets. RMT8 samples were representative of the  
234 macrozooplankton and RMT1 samples were representative of the mesozooplankton (Atkinson and  
235 Peck, 1990; Ward, 1989). A flowmeter (Hydro Bios, Kiel) was mounted in the mouth of the  
236 RMT8 to measure the water volume filtered. Net tows were conducted at a speed of 2 to 2.5 kn.  
237 RMT8 samples were preserved in a 4% formaldehyde and seawater solution. Specimens were  
238 identified to the species level, counted and measured. Dry weight biomass was calculated using  
239 known length-weight relationships (Mizdalski, 1988; E. Pakhomov, *unpublished data*). RMT1  
240 samples were split and one half preserved in a 4% formaldehyde and seawater solution formalin,  
241 and the other half sieved, dried at  $50^\circ\text{C}$  for 48 hours, and weighed for sample dry weight.

## 242 **3. RESULTS**

### 243 ***3.1 Hydrography: Fronts and water masses***

244 Vertical meridional potential temperature ( $\theta$ ), salinity, potential density, oxygen, DFe and Chl-  
245  $a_{\text{FLUO}}$  over the upper 500 m are shown in Figure 1. A detailed description of the hydrographic  
246 characteristics encountered along the 10°E transect is given in Strass et al. (this issue). The Sub-  
247 Antarctic Front (SAF), located at 46.5°S, was identified by an abrupt southward decrease in  
248 surface temperature and salinity. The Antarctic Polar Front (APF), apparent at 49.3°S based on  
249 density profiles, was also associated with the northernmost extent of the temperature minimum  
250 layer. Finally, at 52.5°S, the Southern Polar Front (SPF) was defined by a strong increase in  
251 salinity and steep decrease in surface temperatures.

252 Also indicated in Figure 1 are the water masses sampled along the 10°E transect (Strass et al., this  
253 issue). Antarctic Surface Waters (AASW) and Sub-Antarctic Surface Waters (SASW) occupied  
254 the upper ~100 m south of the SAF. Below the pycnocline, Antarctic Intermediate Water (AAIW),  
255 with its salinity minimum of 34.2, extended northward of the SAF below depths of 300 to 400 m,  
256 whereas Upper Circumpolar Deep Water (UCDW) (salinity = 34.75 and  $\theta = 2^{\circ}\text{C}$ ) was only found  
257 south of the SPF. North of the SAF, a subsurface salinity maximum was evident between 100 and  
258 300 m. This feature likely originated farther north where it was subsequently displaced southward  
259 as an anticyclonic eddy (Strass et al., this issue). Previous observations of such subsurface lobes of  
260 saltier water indicate that this is a common feature of the Subtropical Frontal Zone, located farther  
261 north of this transect (Heath, 1976; Smythe-Wright et al., 1998). Poleward compensation of  
262 Ekman convergence has been suggested as the origin of these features (Heath, 1976), which were  
263 occasionally found as far south as 50°S (Deacon, 1945).

### 264 **3.2 Dissolved iron**

265 DFe concentrations were generally low along the meridional transect, ranging from 0.08 to 0.33  
266 nM in the upper 100 m and varied the major gradients of other ancillary parameters (Figure 1e and  
267 Figure S1). Highest concentrations were measured in the upper 25 m of the SAZ (44°S-46°S)  
268 decreasing southwards, with almost full depletion at ~50°S. This corresponds to the area where the

269 highest Chl-a<sub>FLUO</sub> values were also found (Figure 1f). Indeed, Chl-a<sub>FLUO</sub> and DFe concentrations  
270 were significantly inversely correlated (Spearman correlation coefficient,  $\rho = -0.83$ ,  $p < 0.0001$ ,  $n =$   
271 21).

272 A subsurface increase of DFe was observed at 40 m at the two southernmost stations (81 and 84)  
273 as well as a layer (60-80 m) of depleted DFe (0.07-0.13 nM), that matched a deep Chl-a<sub>FLUO</sub>  
274 maximum ( $\sim 0.6 \text{ mg m}^{-3}$ ) (Figure 1e and 1f). At these same stations below 100 m, higher  
275 concentrations of DFe occurred, which were positively correlated with salinity and negatively  
276 correlated with oxygen (Pearson correlation coefficient,  $r = 0.82$  and  $\rho = -0.85$ , respectively,  $p$   
277  $< 0.01$ ,  $n = 9$ ). Furthermore, these high DFe concentrations were associated with the highest  
278 concentrations of nitrate and phosphate measured along this section ( $> 35 \text{ }\mu\text{M}$  for nitrate and  $> 2.4$   
279  $\mu\text{M}$  for phosphate; data not shown). A subsurface maximum of DFe (80-200 m) was also observed  
280 in the SAZ, coinciding with a subsurface salinity maximum (Figures 1b, 1e).

### 281 3.3 <sup>234</sup>Th deficits and fluxes

282 Significant deficits of <sup>234</sup>Th relative to <sup>238</sup>U (up to  $\sim 45\%$ ) were found in the upper 100-200 m of  
283 the water column at all the stations (Figure 2), with lowest deficiencies ( $\sim 25\%$ ) observed at the  
284 two southernmost stations (52°S and 53°S). Deficits were consistent with the primary production  
285 zone (PPZ), here defined as the depth where fluorescence is reduced to 10% of its maximum value  
286 (Owens et al., 2014; Table 1). No significant <sup>234</sup>Th excess was observed. At 300-350 m, an  
287 additional small depletion of <sup>234</sup>Th was measured at the two southernmost stations. This depletion  
288 was not considered when estimating fluxes at depth due to poor vertical resolution below 200 m.

289 Steady state water column <sup>234</sup>Th fluxes, derived from the integrated <sup>234</sup>Th deficits with respect to  
290 <sup>238</sup>U activities, were determined at three depths at each station (Table 3; Figure 3): i) the  
291 equilibrium depth (Eq. depth; i.e., first depth where there is no significant difference between <sup>238</sup>U  
292 and <sup>234</sup>Th activities within error; Table 1); ii) 100 m, for better comparison with literature values

and to match the shallow ISP deployment depth, and iii) 400 m to match the deep ISP deployment depth and to examine flux attenuation with depth. Fluxes were calculated using a 1-D steady state model (Coale and Bruland, 1985) and neglecting advective and diffusive fluxes. An estimate of the magnitude of these fluxes is provided further below (see section 4.1). The fluxes at 100 m ranged from 1560 to 2610 dpm m<sup>-2</sup> d<sup>-1</sup> (average 2100 ± 400 dpm m<sup>-2</sup> d<sup>-1</sup>). The equilibrium depth was generally found at 150-200 m (except at 52°S and 53°S). These deeper <sup>234</sup>Th deficits represented a 20 - 40% increase in the <sup>234</sup>Th flux estimates, compared to those at 100 m. Thus, <sup>234</sup>Th flux estimates at the equilibrium depth ranged from 1560 to 3570 dpm m<sup>-2</sup> d<sup>-1</sup>, with an average flux of 2600 ± 800 dpm m<sup>-2</sup> d<sup>-1</sup>. Similar fluxes were also obtained at 400 m, ranging from 1320 to 3090 dpm m<sup>-2</sup> d<sup>-1</sup> (average 2300 ± 720 dpm m<sup>-2</sup> d<sup>-1</sup>) (Table 3). <sup>234</sup>Th fluxes estimated at the three depth horizons decreased with latitude ( $r^2 = 0.92$ ,  $p = 0.010$ ;  $r^2 = 0.89$ ,  $p = 0.015$  and  $r^2 = 0.89$ ,  $p = 0.017$ ; for fluxes at 100 m, at equilibrium depth and at 400 m, respectively).

### 3.4 Particulate samples: <sup>234</sup>Th, POC and PON concentrations and ratios

Particulate (>53 µm particle size) <sup>234</sup>Th activities were 1 - 17% of the total <sup>234</sup>Th measured at 100 m, and were between 3-13 times higher than those measured at 400 m (<1% of total <sup>234</sup>Th) (Table 2). POC and PON concentrations were measured in two different filter sets, one where particulate <sup>234</sup>Th was also analyzed (C<sub>Th</sub> and N<sub>Th</sub>) and the other for POC and PON analyses only (C<sub>CN</sub> and N<sub>CN</sub>), to check for heterogeneity in sampling. The POC and PON concentrations measured on both filter sets were similar, validating our measurements on the <sup>234</sup>Th filters used to obtain the C/<sup>234</sup>Th (C<sub>Th</sub>) and N/<sup>234</sup>Th (N<sub>Th</sub>) ratios (C<sub>Th</sub> = 0.91 \* C<sub>CN</sub> + 0.24 and N<sub>Th</sub> = 0.90 \* N<sub>CN</sub> + 0.01;  $r = 0.99$ ,  $p < 0.001$  and  $n = 14$  for both data sets).

POC and PON concentrations (from particles >53 µm) decreased with depth at all the stations (Table 2). C/N ratios remained nearly constant with depth at the two southernmost stations (change <4%), while they varied by a factor of about 2 north of the APF (Table 2). C/<sup>234</sup>Th ratios at 100 m ranged from 11 to 20 µmol C dpm<sup>-1</sup> and from 4.6 to 25 µmol C dpm<sup>-1</sup> at 400 m. North of

the APF, the  $C/^{234}\text{Th}$  ratios at 100 m were higher than the ratios at 400 m. At the southernmost station, at 53°S, the ratio was found to be similar at both depths, and increasing with depth at 52°S (Table 2).  $N/^{234}\text{Th}$  ratios ranged from 1.1 to 3.3  $\mu\text{mol N dpm}^{-1}$  at 100 m and from 0.49 to 4.9  $\mu\text{mol N dpm}^{-1}$  at 400 m. Due to time constraints, ISP could not be deployed at all stations (Figure 1f). Therefore, in order to calculate POC and PON export fluxes at 46°S and 50°S (see section 3.5) we used  $C/^{234}\text{Th}$  and  $N/^{234}\text{Th}$  ratios measured at stations at 44°S and 52°S, which belonged to the same biogeochemical provinces, respectively (44°S and 46°S: SAZ; 50°S and 52°S AZ; Figure 1).

### 3.5 POC and PON fluxes

POC and PON export fluxes were obtained by multiplying the  $^{234}\text{Th}$  fluxes by the  $C(N)/^{234}\text{Th}$  ratios of the particles collected with the ISP (Table 3). These export estimates are therefore based on the assumption that the  $C(N)/^{234}\text{Th}$  ratios of particles  $>53\text{ }\mu\text{m}$  are representative of sinking matter. The rationale for using this conversion factor is that in the SO, large particles, such as diatoms and fecal pellets, are considered to be main drivers of the particulate export flux (Cavan et al., 2015; Honjo et al., 2008; Laurenceau-Cornec et al., 2015; Rutgers van der Loeff et al., 2002). Thus, one would expect particles  $>53\text{ }\mu\text{m}$  to be representative of the sinking material, rather than smaller particle sizes. POC fluxes at 100 m ranged from 25 to 41  $\text{mmol C m}^{-2}\text{ d}^{-1}$ , with no clear latitudinal variation (Figure 3). However, POC export flux estimates at 400 m, indicated enhanced export in the southern half of the transect, whereas at the two northernmost stations significant attenuation of the flux with depth was observed (Table 3; Figure 3). PON fluxes at 100 and 400 m ranged from 2.4 to 7  $\text{mmol N m}^{-2}\text{ d}^{-1}$  and 1.4 to 13  $\text{mmol N m}^{-2}\text{ d}^{-1}$ , respectively, showing similar patterns to the POC fluxes (Table 3). From 44°S to 48°S, POC and PON fluxes at the equilibrium depth tended to be higher than at 100 m, ranging from 34 to 50  $\text{mmol C m}^{-2}\text{ d}^{-1}$  and 3.5 to 9  $\text{mmol N m}^{-2}\text{ d}^{-1}$ , respectively, whereas in the southern half of the transect no significant differences were observed between both depth (Table 3).

### 3.6 Derived primary production

343 Measurements of *in situ* daily primary production using  $^{14}\text{C}$  uptake (PP; see Hoppe et al., this  
344 issue, for details) coincided with  $^{234}\text{Th}$  sampling at only two stations (81 and 84). Therefore, we  
345 used estimated primary production rates (PPRes). PPRes were derived from the relationship  
346 between Chl- $a_{\text{HPLC}}$  standing stock measurements in the upper 100 m of the water column (Chl-  
347  $a_{\text{HPLC\_100m}}$ ) and PP at 100 m from the stations sampled at  $\sim 12^\circ\text{W}$  (from 29 Jan to 17 Feb 2012;  
348 data from Hoppe et al., this issue) and at stations 81 and 84 (C.J.M Hoppe, *unpublished data*):  $\text{PP}$   
349  $= 232 + 13 * \text{Chl-}a_{\text{HPLC\_100m}}$  (with PP expressed in  $\text{mg C m}^{-2} \text{ d}^{-1}$ ;  $r^2 = 0.82$ ,  $p < 0.001$ ,  $n = 11$ ).  
350 Using this equation, PPRes estimated for all stations had a mean relative deviation of -3% and a  
351 standard deviation of 20% when compared to directly measured PP ( $n = 11$ ). The derived PPRes  
352 ranged from 54 to 86  $\text{mmol C m}^{-2} \text{ d}^{-1}$  (Table 3). The stations north of the APF showed  
353 significantly lower PPRes than in the southern half of the transect ( $56 \pm 3 \text{ mmol C m}^{-2} \text{ d}^{-1}$  vs  $78 \pm$   
354  $7 \text{ mmol C m}^{-2} \text{ d}^{-1}$ ).

### 355 **3.7 Phytoplankton and zooplankton distribution**

356 Along the transect, a clear shift in phytoplankton communities was observed north and south of  
357 the APF (Figure 6a, see also Cheah et al., this issue). Nanophytoplankton dominated north of the  
358 APF, with microphytoplankton abundances  $< 40\%$ . South of the APF the phytoplankton  
359 community was dominated by microphytoplankton ( $> 60\%$ ). Picophytoplankton represented  $< 10\%$   
360 along the entire transect.

361 Total mesozooplankton biomass was an average of 45% higher than macrozooplankton biomass  
362 across the transect (Figure 6b). An exception was at  $52^\circ\text{S}$  where the macrozooplankton biomass  
363 was inflated by a large ctenophore catch. Mesozooplankton biomass was elevated in the vicinity of  
364 the APF, but no clear difference was observed between the areas to the north and south of this  
365 front. Macrozooplankton biomass tended to be higher south of the APF, but stations with  
366 comparable biomass were recorded north of the APF. Overall, the macroplankton community  
367 north of the APF was dominated (in order of numerical importance) by chaetognaths (54%), while



368 south of the APF salps accounted for up to 91% of the numerical abundance (Figure 6c). A  
369 detailed description of the zooplankton composition is presented in Hunt and Pakhomov (this  
370 issue).

#### 371 4. DISCUSSION

372 The SO has been previously described as “one of the ocean’s most efficient biological pumps”  
373 (Buesseler et al., 2001), although it has recently been suggested that on a global scale, its carbon  
374 export potential might be lower than previously thought (Maiti et al., 2013). High POC export  
375 fluxes ( $>20 \text{ mmol C m}^{-2} \text{ d}^{-1}$ ) occurring in late austral spring/summer following phytoplankton  
376 blooms have been observed repeatedly (Buesseler et al., 2003; Friedrich and Rutgers van der  
377 Loeff, 2002; Savoye et al., 2008). Our estimates of  $^{234}\text{Th}$  fluxes at 100 m ( $1560 \text{ to } 2610 \text{ dpm m}^{-2} \text{ d}^{-1}$ )  
378 are within the mid to upper range of previously reported estimates (from negligible to  $3800 \text{ dpm m}^{-2} \text{ d}^{-1}$ ;  
379 on average  $1660 \pm 920 \text{ dpm m}^{-2} \text{ d}^{-1}$ ,  $n = 201$ ; Figure 4). Our Th-derived POC fluxes  
380 estimated along the  $10^\circ\text{E}$  transect ( $25 \text{ to } 41 \text{ mmol C m}^{-2} \text{ d}^{-1}$ ) are, however, among the highest  
381 fluxes reported to date within the SO (from negligible to  $91 \text{ mmol C m}^{-2} \text{ d}^{-1}$ ; on average  $13 \pm 13$   
382  $\text{mmol C m}^{-2} \text{ d}^{-1}$ ;  $n = 273$ ; Figure 4; also see compilations by Maiti et al., 2013 and Le Moigne et  
383 al., 2013), and close to values found in areas with natural and artificially high iron inputs (e.g.,  
384 Morris et al., 2007; Smetacek et al., 2012). This is surprising given that our measurements were  
385 conducted in open ocean areas of the ACC. In the following sections, the effects of physical  
386 processes are investigated in order to validate the 1-D steady state approach applied (section 4.1).  
387 The distribution of DFe is discussed relative to previous studies and with  $^{234}\text{Th}$  activity profiles.  
388 Biological uptake and possible inputs linked to water masses are also explored (section 4.2).  
389 Variability in export along the transect is also examined in light of planktonic community  
390 structure in order to provide insight into the main drivers of POC export fluxes throughout the  
391 region (section 4.3), and how differences in food webs may affect POC export and transfer  
392 efficiencies to depth (section 4.4). Finally, a comparison with previous studies is also presented to

393 highlight the large variability within the SO, mainly linked to the timing and magnitude of the  
394 phytoplankton blooms (section 4.5).

#### 395 ***4.1 Physical transport processes: effect on $^{234}\text{Th}$ export fluxes***

396 Steady-state conditions were assumed to calculate  $^{234}\text{Th}$  export fluxes as none of the stations were  
397 revisited during the expedition. Previous studies have shown export fluxes to be relatively  
398 constant over time in the study area during the austral summer, with no significant differences  
399 between results obtained when applying steady and non-steady state conditions (Rutgers van der  
400 Loeff et al., 2011, 2002). In general, in the open ocean, diffusion and advection are considered to  
401 be negligible compared to the vertical downward flux of  $^{234}\text{Th}$  on sinking particles (see review by  
402 Savoye et al., 2006) except in strong upwelling areas (Buesseler et al., 1998). However, the study  
403 area is located in a dynamic region characterized by three fronts where advective and diffusive  
404 processes could be significant (Strass et al., this issue). For instance, Strass et al. (2002b) reported  
405 mesoscale frontal dynamics that influenced chlorophyll distribution patterns, which were highly  
406 correlated with other biological parameters, such as primary production (Strass et al., 2002a) and  
407 zooplankton abundances (Pollard et al., 2002a). Therefore, we assessed the assumption of  
408 negligible physical processes on our  $^{234}\text{Th}$  flux calculations (see details in the supplementary  
409 information). Our estimates indicate that, overall, the combination of advective and diffusive  
410 fluxes would represent 7 - 17% of the  $^{234}\text{Th}$  export fluxes at 100 m, comparable to their associated  
411 uncertainties (6 - 12%). Therefore, by taking into account physical transport mechanisms, the  
412 uncertainty of  $^{234}\text{Th}$  export fluxes would increase to 10-21%, in agreement with previous results  
413 presented by Resplandy et al. (2012), where errors due to the dynamic transport of  $^{234}\text{Th}$  related to  
414 small-scale structures were found to be < 20%.

#### 415 ***4.2 Dissolved Fe distributions***

416 The distribution of Chl-a in the SO is mainly regulated by inputs of new iron to the system

417 (Sokolov and Rintoul, 2007). DFe concentrations in the Atlantic sector of the ACC progressively  
418 decrease eastwards as the ACC moves from the main iron source (the Antarctic Peninsula and  
419 South Georgia, de Jong et al., 2012). Despite the high spatial variability shown here, our DFe data  
420 are in excellent agreement with the few prior sampling efforts carried out in this sector of the SO  
421 (Figure S1) (Chever et al., 2010; Klunder et al., 2011) suggesting that major features in DFe  
422 distributions are persistent during the austral summer.

423 Satellite images show high Chl-a concentrations (up to  $1.3 \text{ mg m}^{-3}$ ) north of the APF about a  
424 month prior to the cruise (Figure 5; Figure S2). However, DFe concentrations in that area were not  
425 as depleted as in the central region of the transect during the cruise (Figure 1e). The biological  
426 uptake of DFe north of the APF might have been limited by silicate availability since silicate  
427 concentrations were in the range of limiting concentrations, namely  $\leq 1 \text{ } \mu\text{M}$  (Figure 7) (Le  
428 Moigne et al., 2013a, Cheah et al., this issue). Additionally, the high salinity intrusion at 100-300  
429 m supports a lateral advection of DFe (Figures 1b and 1e). During the cruise, the highest Chl-a  
430 concentrations (up to  $1.2 \text{ mg m}^{-3}$ ; Figure S1) were measured between  $49^{\circ}\text{S}$  and  $52^{\circ}\text{S}$  (Figure 5e),  
431 leading to strong depletion of DFe in the upper 100 m. The low DFe values were probably caused  
432 by recent biological uptake and the subsequent removal through sinking particles. Biological  
433 uptake of DFe would explain its inverse correlation with  $\text{Chl-a}_{\text{FLUO}}$  ( $\rho = -0.83$ ,  $p < 0.0001$ ,  $n = 21$ ).  
434 In general, DFe and  $^{234}\text{Th}/^{238}\text{U}$  profiles followed a similar trend with depth, and are inverse to Chl-  
435  $\text{a}_{\text{FLUO}}$  profiles, with DFe depletion matching the increase of  $^{234}\text{Th}$  deficits (Figure S1). This  
436 suggests that the process causing the reduction of DFe concentrations also affected the  $^{234}\text{Th}$   
437 deficits at a similar depth range. However, it should be noted that the gradient in  $^{234}\text{Th}$  deficits are  
438 steeper than gradients in DFe (between  $\sim 60 - 200 \text{ m}$ ), probably due to a more rapid turnover of Fe  
439 than that of  $^{234}\text{Th}$ , a finding also reported by Klunder et al. (2011).

440 The highest DFe concentrations were found in the southern part of the transect (St. 81 and 84),  
441 below  $\sim 300 \text{ m}$  associated with UCDW waters, where oxygen concentrations were ( $< 200 \text{ } \mu\text{mol kg}^{-1}$

1) (Figure 1d). Indeed, DFe concentrations below 100 m were strongly correlated with salinity and negatively correlated with oxygen at those two stations ( $\rho = 0.88$  for salinity and  $\rho = -0.85$  for oxygen, with  $p < 0.01$  and  $n = 9$  for both correlations). Higher DFe concentrations have been found previously in UCDW waters (Klunder et al., 2011) and are typical of reduced oxygen concentrations due to an increase of iron solubilization during POC remineralization and stabilization of highly soluble Fe(II) (Millero et al., 1987). Low Chl-a<sub>FLUO</sub> values despite high concentrations of all major nutrients at the southern end of the transect (Figure 7) indicate, however, that little of the DFe in UCDW waters reaches the photic layer.

#### 4.3 Differences in planktonic community N-S of the APF: Effects on POC export and attenuation

SO fronts are physical boundaries that delimit zones of distinct physical, chemical, and biological properties (e.g., Read et al., 2002; Strass et al., 2002b) that in turn could regulate the particle export flux. In this study we did not observe a clear zonation related to the fronts regarding  $^{234}\text{Th}$  export fluxes, although enhanced export was measured in areas where, as indicated by satellite imagery (Figure 5, Figure S2), phytoplankton blooms occurred and peaked about a month prior to our sampling (north of the APF). Since the  $^{234}\text{Th}$  method integrates over time scales of several weeks, we could expect a decoupling between  $^{234}\text{Th}$  deficiencies in the upper water column as compared to the biological parameters measured during the cruise (e.g., Chl-a concentrations or primary production) (Buesseler, 1998).

The POC export fluxes at 100 m were in the higher end of the range of previous reported estimates, mainly driven by high  $C/^{234}\text{Th}$  ratios (Figure 4). Further, contrary to  $^{234}\text{Th}$  fluxes, POC fluxes were not correlated with latitude ( $r^2 = 0.27$ ;  $p = 0.29$ ; similar for PON fluxes:  $r^2 = 0.08$ ;  $p = 0.59$ ) (Figure 3). Differences between stations north and south of the APF were found when comparing changes in POC export fluxes at 100 and 400 m. Due to changes in  $C/^{234}\text{Th}$  ratios with depth, POC fluxes between 100 and 400 m depth showed higher attenuation north of the APF than

southern stations, which showed little to no attenuation (Figure 3; Table 3). C content in particles varies due to particle volume and composition, whereas  $^{234}\text{Th}$  is quickly adsorbed onto the particles' surface sites (Santschi et al., 2006). As a consequence, first order dynamics predicts an increase in C/ $^{234}\text{Th}$  ratio in large particles due to high volume:surface area ratios (Buesseler et al., 2006). However, additional aspects of the biological community (e.g., dominant phytoplankton group, bacterial activity, grazing, nutrient limitation) may also affect C content and C/ $^{234}\text{Th}$  ratios in particles and their variation with depth (Buesseler et al., 2006; Jacquet et al., 2011; Puigcorb  et al., 2015), leading to the large variability in C/ $^{234}\text{Th}$  ratios in particles (Figure 4; Buesseler et al., 2006). Below we discuss the differences encountered north and south of the APF and their impact on the POC export flux and attenuation (Table 4 summarizes the comparison between stations north and south of the APF).

#### *4.3.1 North of the APF: small phytoplankton and higher particle attenuation*

In accordance with nutrient distribution (low Si north of the APF and low nitrate and phosphate north of the SAF; Figure 7) planktonic communities north of the APF were dominated by nanophytoplankton (mainly haptophytes; Cheah et al., this issue and Figure 6a) and had higher abundances of carnivorous zooplankton (Hunt et al., this issue and Figure 6c). In this half of the transect, a bloom took place a month prior to the sampling period (Figure 5; Figure S2). The higher POC:Chla ratios found north of the APF also reflect communities in a later stage of development with a larger fraction of heterotrophs or detritus (Figure 6d). Since the  $^{234}\text{Th}$  approach integrates over a period of time of a few weeks, the important  $^{234}\text{Th}$  deficits observed at the northern stations were most probably a consequence of that bloom, which might have been dominated by larger phytoplankton groups, such as diatoms. However, during the sampling time (post-bloom conditions), the small size of the dominant phytoplankton group (<20  $\mu\text{m}$ ), combined with the lack of dense frustules and skeletons associated with diatoms, probably led to the formation of a sinking particulate pool also dominated by small and more slowly sinking particles. Both processes would allow more remineralization, which might explain the larger attenuation of

493 POC and  $^{234}\text{Th}$  fluxes and  $\text{C}/^{234}\text{Th}$  ratios with depth in the northern half of the transect. The  
494 differences observed in C/N ratios with depth at both stations also suggest alteration of the particle  
495 composition with depth (Table 2). Overall, POC flux attenuation was observed north of the APF,  
496 with up to a 74% decrease in flux between equilibrium depth and 400 m, although it should be  
497 noted that vertical resolution below 200 m was poor.

#### 498 4.3.2 South of the APF: large phytoplankton and low attenuation

499 In the southern half of the transect, south of the APF, higher nitrate and silicate concentrations  
500 (Figure 7) favored larger phytoplankton, in particular diatoms (Figure 6a; Cheah et al., this issue).  
501 The higher POC standing stocks combined with lower POC/Chl-a ratios (Figure 6d) indicate that  
502 communities south of the APF had a higher proportion of phytoplankton relative to that observed  
503 towards the north, where the bloom had occurred a month prior to our expedition (Figure 5). The  
504 southern region was also likely subject to more intense grazing pressure due to higher abundances  
505 of herbivorous zooplankton, mostly salps (Figure 6c). Pigment analyses also suggest that grazing  
506 took place at those latitudes (Cheah et al., this issue). The structure of the diatom dominated  
507 planktonic community in this area (including thickly silicified species characteristic of iron  
508 deficient open ocean areas of the Southern Ocean; Assmy et al., 2013) and abundance of salps,  
509 might have led to both retention of POC at the surface (Assmy et al., 2013; Iversen et al., this  
510 issue) as well as production of a sinking particle pool constituted by large fast sinking particles  
511 that were rapidly able to reach 400 m and only be minimally affected by remineralization (Rutgers  
512 van der Loeff et al., 2002). Salps were 2-3 orders of magnitude more abundant at the southern  
513 stations compared to northern stations (B.P.V. Hunt, *pers. comm.*). These large grazers can  
514 produce fast sinking fecal pellets ( $200\text{--}2700\text{ m d}^{-1}$ , Bruland and Silver, 1981; Iversen et al., this  
515 issue; Madin, 1982; Phillips et al., 2009; Turner, 2002) and have rapid defecation rates (Madin,  
516 1982), making them potentially important contributors to POC export (Ebersbach and Trull, 2008;  
517 Perissinotto and Pakhomov, 1998; Phillips et al., 2009; Smith et al., 2013). The additional  
518 ballasting due to the inclusion of thickly silicified diatoms, such as *Fragilariopsis kerguelensis*

519 which dominated assemblages at station 84 (53°S; Klaas, *unpublished*), may also increase the  
520 sinking velocities of fecal pellets and aggregates (Francois et al., 2002; Klaas and Archer, 2002),  
521 reducing their residence time in the upper ocean. This could help explain the small variation of the  
522 C/N ratios and low/negligible POC flux attenuation with depth at the southernmost stations (Table  
523 2).

524 Additional information regarding POC export south of the APF is derived from surface tethered  
525 sediment traps deployed at 53°S, at 100 and 400 m (Iversen *et al.*, *unpublished data*). Differences  
526 between both techniques (from water column  $^{234}\text{Th}$  deficits versus POC export measured directly  
527 from the sediment traps) are typically found in the literature to be within a factor of 2 to 4, partly  
528 due to their time scale of collection (several weeks *vs* ~24 h), as well as methodological issues  
529 between techniques (Buesseler, 1991). As such, both methods can be used to complement one  
530 another. The particulate C/ $^{234}\text{Th}$  ratios collected using sediment traps were about a factor of 3  
531 lower than those collected using ISP, although similar to ISP, the ratio did not change with  
532 increasing depth ( $6.5 \pm 0.5$  and  $6.9 \pm 0.6 \mu\text{mol C dpm}^{-1}$ , at 100 and 400 m, respectively).  
533 Sediment trap particles also contained a large presence of fecal pellets (MH. Iversen, *pers.*  
534 *comm.*). While the lack of a change in C/ $^{234}\text{Th}$  ratios confirms the results obtained for ISP particles  
535 ( $>53\mu\text{m}$ ), the differences in magnitude of the C/ $^{234}\text{Th}$  ratios suggest that the POC fluxes estimated  
536 using ISP particles represent an upper limit, at least at 53°S. POC fluxes measured by sediment  
537 traps at 53°S (MH. Iversen *pers. comm.*) also show small flux attenuation with depth (36% and  
538 11%, for sediment traps and the  $^{234}\text{Th}$  method, respectively), again confirming the results obtained  
539 with the  $^{234}\text{Th}$  approach.

#### 540 **4.4 Export and transfer efficiencies**

541 Numerous studies have reported significant carbon export from the upper water column in the SO  
542 based on a variety of methodological approaches (e.g., oxygen or nutrient mass balance, short-  
543 lived radionuclides, sediment traps) and across different frontal regions (Buesseler et al., 2001;

544 Cochran et al., 2000; Friedrich and Rutgers van der Loeff, 2002; Hoppema et al., 2002; Rutgers  
545 van der Loeff et al., 1997; Savoye et al., 2008; Schlitzer, 2002; Usbeck et al., 2003) and  
546 productivity systems (Cavan et al., 2015; Ebersbach et al., 2011; Manno et al., 2015; Rembauville  
547 et al., 2015a, 2015b; Salter et al., 2012). The overall emerging picture from these studies suggest  
548 that in areas with high productivity downward transport of organic carbon is mainly driven by  
549 blooms of diatoms (leading to the export of 30-50% of SO net primary production) with  
550 zooplankton fecal material as a major pathway for exporting carbon to the deep ocean after the  
551 major sedimentation pulse (diatom dominated spring bloom) in areas with low productivity  
552 (Cavan et al., 2015; Laurenceau-Cornec et al., 2015; Manno et al., 2015; Rembauville et al.,  
553 2015a)

554 In this study, export efficiencies were calculated by dividing the Th-derived POC fluxes at 100 m  
555 by the PPRes. Higher export efficiencies were coincident with lower PPRes, i.e., north of the APF  
556 (Table 3), similar to the results previously reported by Lam and Bishop, (2007), Maiti et al. (2013)  
557 and Laurenceau-Cornec et al. (2015). Using the equation of Maiti et al., (2013) to obtain the  
558 export efficiencies based on the PP ( $\text{Export efficiency} = -0.3482 * \log(\text{PP}) + 1.2239$ ; Figure 3a in  
559 Maiti et al., 2013) we found good agreement with our data at stations 44°S and 46°S (ratios  
560 between measured and derived export efficiency of 1.1 and 1.0, respectively), whereas for the  
561 other stations, lower export efficiencies than predicted by the model of Maiti et al. (2013) were  
562 obtained (average ratio between both estimates  $0.71 \pm 0.07$ ;  $n = 4$ ). The decoupling between the  
563 peak of the productive period (before the cruise) and the timing of export (declining of productive  
564 period; during the cruise) could be responsible for the higher export efficiencies (average 60%,  
565 range 46-69%) measured north of the APF. Rutgers van der Loeff et al. (1997) found similar  
566 results during an austral spring bloom where there was also a delay between the increase in  
567 phytoplankton standing stocks and  $^{234}\text{Th}$  depletion, similar to Buesseler et al. (2003), who reported  
568 a delay between onset of production and export of up to 1 month. Export efficiencies south of the



APF were lower (max. 44%). A relatively small export efficiency (27%) was also confirmed south of the APF using sediment trap results deployed at 53°S (MH. Iversen, *pers. comm.*).

Stations south of the APF, however, had the highest transfer efficiencies (i.e., the percentage of POC flux at the equilibrium depth that reaches 400 m), ranging between 89% and 148% (Table 3). As discussed previously, these high transfer efficiencies can be explained by fast-sinking and weakly attenuated sinking material, combined with the effect of diel vertical migration of zooplankton (Cavan et al., 2015). Alternatively, these high transfer efficiency might be due to an overestimate of our  $C/^{234}\text{Th}$  ratios based on particles  $>53\ \mu\text{m}$  (not necessarily sinking particles). Differences in attenuation are, however, primarily due to the fact that, in strong contrast to stations north of the APF,  $C/^{234}\text{Th}$  ratios south of the APF do not change with depth.  $C/^{234}\text{Th}$  ratios in sediment trap material (measured only at 53°S), although lower than the ratios obtained from ISP, also present no decrease with depth. A comparison of  $C/^{234}\text{Th}$  ratios from several trap deployments south of the APF during the same cruise (Roca-Martí et al., this issue) did not show a systematic bias for  $C/^{234}\text{Th}$  ratios for ISP collected material compared to trap collected material. Further, no large differences were observed in  $C/^{234}\text{Th}$  ratios between 100 m and 300 m, similar to our results. In Roca-Martí et al. (this issue), Chl-a and fucoxanthin were found to be efficiently transferred between 100 and 300 m indicating that these pigments were exported to 300 m with little to no breakdown. Results from Cedhagen et al. (2014), obtained during the same expedition, also corroborate these findings as large concentrations of algal pigments were observed in the cytoplasm of foraminifera collected at depths  $>4000\ \text{m}$ . Moreover, at station 81 (52°S;  $\sim 3500\ \text{m}$  depth), Ruff et al. (2014) observed a large number of diatom frustules and intact fecal pellets in the top layers of the sediments, even down to 5 cm depth. Combined these studies suggest rapid transport of material to sediments using a variety of pathways.

#### 4.5 Comparison with previous studies

A global compilation of  $^{234}\text{Th}$ -derived POC export estimates by Le Moigne et al. (2013), available

594 in <http://doi.pangaea.de/10.1594/PANGAEA.809717>, contains a number of studies located in the  
595 SO (iron fertilization experiments not included). Considering all these studies together with the  
596 results from our expedition presented here and in Roca-Martí et al. (this issue), as well as  
597 Planchon et al. (2015), Rosengard et al. (2015) and Savoye et al. (2008), we observed wide ranges  
598 in  $^{234}\text{Th}$  export fluxes and  $\text{C}/^{234}\text{Th}$  ratios, with subsequent variability in the derived POC fluxes at  
599  $100 \pm 10$  m depth (Figure 4). This compilation, however, includes a variety of areas that are  
600 difficult to compare with our open ocean stations due to the large differences in phytoplankton  
601 assemblage and growth and biogeochemical aspects linked to their geographical location (e.g., ice  
602 coverage or Fe inputs from continental shelves). Therefore, here we only discuss our results  
603 together with studies conducted in the Atlantic sector of the open ACC (between  $40^\circ\text{S}$ - $60^\circ\text{S}$  and  
604  $15^\circ\text{E}$ - $15^\circ\text{W}$ ; see map inset in Figure 4) namely Planchon et al. (2013), Roca-Martí et al. (this  
605 issue), Rutgers van der Loeff et al. (2011, 2002, 1997) and Smetacek et al. (2012), outside the iron  
606 fertilization patch.

607 Except for the SO-JGOFS expedition (Rutgers van der Loeff et al., 1997), which was conducted  
608 during the austral spring (Oct-Nov 1992;  $6^\circ\text{E}$ ), all the studies discussed here were conducted  
609 during the austral summer (Dec-Jan) or late austral summer (Feb-Mar). During the austral spring,  
610 short but intense bloom events seem to contribute significantly to the annual C export. Data in  
611 Rutgers van der Loeff et al. (1997) supports this observation with a maximum  $^{234}\text{Th}$  export flux of  
612  $3250 \text{ dpm m}^{-2} \text{ d}^{-1}$  at 100 m during a productive period of only 22 days and a POC flux at 100 m  
613 ranging from 19 to  $38 \text{ mmol C m}^{-2} \text{ d}^{-1}$ , similar to the results observed during our study. Rutgers  
614 van der Loeff et al. (2002) reported constant export fluxes during a two week period of the austral  
615 summer three years later (1995/96).  $^{234}\text{Th}$  and POC export fluxes at 100 m were  $865 \text{ dpm m}^{-2} \text{ d}^{-1}$   
616 and  $8.8 \text{ mmol C m}^{-2} \text{ d}^{-1}$ , respectively. The magnitude of the fluxes presented by Rutgers van der  
617 Loeff et al. (2002) is similar to those reported by Planchon et al. (2013) during the Bonus  
618 GoodHope (BGH) expedition (Feb-Mar 2008), ranging from  $870$  to  $1200 \text{ dpm m}^{-2} \text{ d}^{-1}$  and  $2.3$  to  
619  $5.1 \text{ mmol C m}^{-2} \text{ d}^{-1}$  for the section of their transect between  $44^\circ\text{S}$  and  $53^\circ\text{S}$ . This is almost 3 times

620 lower in  $^{234}\text{Th}$  fluxes and about an order of magnitude smaller POC export fluxes than the  
621 estimates calculated in our study. Rutgers van der Loeff et al. (2011) reported  $^{234}\text{Th}$  fluxes along  
622 the prime meridian (Feb 2008) that also decreased with increasing latitude, and were up to 1.6  
623 times lower than the export fluxes from the current study at similar locations with respect to the  
624 frontal systems. The maximum POC export fluxes estimated by Rutgers van der Loeff et al.  
625 (2011) were  $11 \text{ mmol C m}^{-2} \text{ d}^{-1}$  using the bulk of particles to obtain  $\text{C}/^{234}\text{Th}$  ratios, although this  
626 value decreases by a factor of 2 when using  $>50 \text{ }\mu\text{m}$  particles ( $5.4 \text{ mmol C m}^{-2} \text{ d}^{-1}$ ). The  
627 differences between both estimates highlight the importance that the particle composition has on  
628  $\text{C}/^{234}\text{Th}$  ratios and the necessity of properly sampling the particles that are contributing to the  
629 export flux, which is still an open topic of discussion (Bishop et al., 2012; Durkin et al., 2015;  
630 Puigcorb  et al., 2015). Smetacek et al. (2012) examined  $^{234}\text{Th}$  and Th-derived POC fluxes outside  
631 an iron fertilized patch (Feb-Mar 2004), with  $\sim 1600\text{-}2500 \text{ dpm m}^{-2} \text{ d}^{-1}$  and  $\sim 32\text{-}41 \text{ mmol C m}^{-2} \text{ d}^{-1}$ ,  
632 close to the values reported here. Finally, Roca-Mart  et al. (this issue) provide results from a  
633 bloom at  $\sim 12^\circ\text{W}$  and  $\sim 51^\circ\text{S}$  during our expedition, where average  $^{234}\text{Th}$  and Th-derived POC  
634 export fluxes at 100 m were  $2390 \pm 340 \text{ dpm m}^{-2} \text{ d}^{-1}$  ( $n = 14$ ) and  $36 \pm 15 \text{ mmol C m}^{-2} \text{ d}^{-1}$  ( $n = 9$ ),  
635 respectively.

636 The results from the 2012 Eddy-Pump survey presented here and in Roca-Mart  et al. (this issue)  
637 are comparable to the spring bloom export presented in Rutgers van der Loeff et al. (1997) and  
638 also with the summer fluxes estimated by Smetacek et al. (2012) outside of the iron fertilized  
639 patch. The main factor driving the differences between POC flux estimates are the  $\text{C}/^{234}\text{Th}$  ratios,  
640 which were much lower during the 2008 expeditions (ranging from 1.7 to  $4.8 \text{ }\mu\text{mol C dpm}^{-1}$ )  
641 (Planchon et al., 2013 and Rutgers van der Loeff et al., 2011) than the ratios measured during this  
642 study ( $16 \pm 4 \text{ }\mu\text{mol C dpm}^{-1}$ ), in Roca-Mart  et al. (this issue) ( $14 \pm 3 \text{ }\mu\text{mol C dpm}^{-1}$ ) and in  
643 Smetacek et al. (2012) ( $17 \pm 3 \text{ }\mu\text{mol C dpm}^{-1}$ ).

644 As previously discussed, the planktonic community structure will affect the type and composition

645 of the particles generated in surface layers. Thus, the sampling time related to a bloom event (i.e.,  
646 sampling prior, during or after a bloom) can lead to differences in the C/<sup>234</sup>Th ratios measured.  
647 High Chl-a concentrations (>1 mg m<sup>-3</sup>) covering large areas can be observed from satellite images  
648 during the sampling period of this expedition (Jan-Feb 2012; see also Figure 1 in Hoppe et al., this  
649 issue) and in Smetacek et al. (2012), prior to iron fertilization. These features were minimal and  
650 mainly located further west in Jan-Feb 2008 (see Figure 7 in Rutgers van der Loeff et al., 2011).  
651 As suggested by Planchon et al. (2013) and Rutgers van der Loeff et al. (2011), the low fluxes  
652 obtained during the 2008 expeditions were probably due to a post-bloom situation, where the  
653 intensive export had already occurred and remineralization led to reduced POC export fluxes. Our  
654 study was carried on earlier in the summer, probably during the late export phase where  
655 remineralization is not able to compensate the <sup>234</sup>Th deficits created by the still present particle  
656 export. Additionally, comparison between summers 2007/2008 and 2011/2012 using satellite  
657 images (Figure S2) suggests that the higher export fluxes measured during 2012 were probably not  
658 only a consequence of the sampling time but also due the larger magnitude of the bloom of that  
659 year. Thus, not only the timing of sampling relative to the bloom, but also its magnitude, can  
660 result in clearly different estimates of POC export fluxes, mainly due to the variability in the  
661 C/<sup>234</sup>Th ratios, even during the austral summer.

## 662 5. CONCLUSIONS

663 In this study, <sup>234</sup>Th was used as a tracer to estimate downward particle fluxes across the ACC in  
664 order to examine the effect of hydrographic conditions, separated by fronts, on POC export, export  
665 efficiencies and transfer efficiencies. <sup>234</sup>Th fluxes were higher in the northern part of the 10°E  
666 transect, due to a bloom that occurred about a month before our arrival, as revealed by satellite  
667 images. POC fluxes at 100 m were relatively high (25 to 41 mmol C m<sup>-2</sup> d<sup>-1</sup>) and did not show  
668 significant differences linked to the frontal zones. However, a major N-S shift in planktonic  
669 community was reflected in the variation of the C/<sup>234</sup>Th ratios with depth. Small phytoplankton

670 with low Chl-a concentrations dominated the transect north of the APF, whereas south of the APF  
671 diatoms dominated the phytoplankton community, Chl-a was higher, and salps dominated the  
672 macrozooplankton community. This probably resulted in sinking particle pools that differed in  
673 their composition: aggregates of small particles in the north versus fast-sinking large particles in  
674 the south. Export efficiencies were generally high (35 - 69%) partly due to a temporal decoupling  
675 between production and export, with slightly higher values in the northern section, where derived  
676 primary production rates were found to be lower and small phytoplankton dominant. On the other  
677 hand, due to the absence of attenuation of the  $C/^{234}\text{Th}$  ratios with depth at the southern stations,  
678 POC fluxes at 400 m were similar or even higher than at 100 m, which translates to high transfer  
679 efficiencies in the region where diatoms and salps were more abundant.

680 Comparison with previous studies highlights the dynamic biological character of the study area,  
681 with phytoplanktonic blooms of different magnitude that, together with the time elapsed between  
682 the climax of the bloom and the sampling period, probably led to the differences observed  
683 between studies, where large variability regarding  $C/^{234}\text{Th}$  ratios was observed. This supports the  
684 use of combined techniques, such as sediment traps and the  $^{234}\text{Th}$ -method, to estimate the  
685 magnitude and composition of particle fluxes. Further efforts should be made in order to link the  
686 planktonic community to variability of  $C/^{234}\text{Th}$  ratios, not just below the euphotic zone but also at  
687 greater depths, in order to constrain the strength and efficiency of the biological pump in this  
688 region.

689

## 690 **Acknowledgments**

691 We are grateful to the crew of R/V *Polarstern*, the chief scientist of the cruise Dieter Wolf-  
692 Gladrow and the scientists on board for their cooperation and assistance during the cruise. We  
693 further thank the members of the oceanography team, Harry Leach, Harmut Prandke, Matthew

694 Donnelly and Matthias Krüger, for providing the hydrographical data. We wish to acknowledge  
695 Matthew Donnelly for the help with the in situ pump sampling, Ingrid Stimac for her assistance  
696 with the cruise preparation and ICPMS analyses, Mariana Soppa for help on board with pigment  
697 sampling and Sonja Wiegmann for HPLC analysis. We thank Morten H. Iversen for making  
698 available sediment trap data. We are really grateful for Joan Llor, Peter Strutton and Tom Trull  
699 contributions to the discussion of the data. Thanks also to the European Space Agency (ESA) for  
700 OC-CCI and MERIS data and NASA-GFSC for MODIS and SeaWiFS data. Financial support for  
701 this project was provided by the Ministerio de Ciencia e Innovación (CTM2011-14027-E, Spain)  
702 and the Generalitat de Catalunya to the research group MERS (2014 SGR-1365). VP and MRM  
703 have been funded by Ph.D. Fellowships from the Spanish government (AP-2009-4733 and  
704 AP2010-2510, respectively). The participation of LML and JSE was funded by the MINECO of  
705 Spain (CGL2010-11846-E). Funding to WC and AB was supplied partly by the Helmholtz  
706 Innovation Fund Phytooptics. MH was partly supported by the DFG in the framework of the  
707 priority programme "Antarctic Research with comparative investigations in Arctic ice areas" by a  
708 grant HO 4680/1.

709

## 710    **References**

- 711    Arrigo, K.R., Worthen, D., Schnell, A., Lizotte, M.P., 1998. Primary production in Southern  
712        Ocean waters. *J. Geophys. Res.* 103, 600,15515–15587.
- 713    Assmy, P., Smetacek, V., Montresor, M., Klaas, C., Henjes, J., Strass, V.H., Arrieta, J.M.,  
714        Bathmann, U., Berg, G.M., Breitbarth, E., Cisewski, B., Friedrichs, L., Fuchs, N., Schüller,  
715        S.E., Steigenberger, S., Webb, A., Wolf-Gladrow, D., 2013. Thick-shelled, grazer-protected  
716        diatoms decouple ocean carbon and silicon cycles in the iron-limited Antarctic Circumpolar  
717        Current. *Proc. Natl. Acad. Sci.* 110, 20633–20638. doi:10.1073/pnas.1309345110
- 718    Atkinson, A., Peck, J.M., 1990. The distribution of zooplankton in relation to the South Georgia  
719        shelf in summer and winter, in: *Antarctic Ecosystems*. Springer, pp. 159–165.
- 720    Aumont, O., Bopp, L., 2006. Globalizing results from ocean in situ iron fertilization studies.  
721        *Global Biogeochem. Cycles* 20, GB2017. doi:10.1029/2005GB002591
- 722    Barlow, R.G., Cummings, D.G., Gibb, S.W., 1997. Improved resolution of mono- and divinyl  
723        chlorophylls a and b and zeaxanthin and lutein in phytoplankton extracts using reverse phase  
724        C-8 HPLC. *Mar. Ecol. Prog. Ser.* 161, 303–307.
- 725    Benitez-Nelson, C., Buesseler, K.O., Rutgers van der Loeff, M., Andrews, J., Ball, L., Crossin, G.,  
726        Charette, M.A., 2001. Testing a new small-volume technique for determining <sup>234</sup>Th in  
727        seawater. *J. Radioanal. Nucl. Chem.* 248, 795–799.
- 728    Bishop, J.K.B., Lam, P.J., Wood, T.J., 2012. Getting good particles: Accurate sampling of  
729        particles by large volume in-situ filtration. *Limnol. Oceanogr. Methods* 10, 681–710.  
730        doi:10.4319/lom.2012.10.681
- 731    Boyd, P.W., Jickells, T., Law, C.S., Blain, S., Boyle, E.A., Buesseler, K.O., Coale, K.H., Cullen,  
732        J.J., de Baar, H.J.W., Follows, M., Harvey, M., Lancelot, C., Levasseur, M., Owens, N.P.J.,  
733        Pollard, R., Rivkin, R.B., Sarmiento, J., Schoemann, V., Smetacek, V., Takeda, S., Tsuda, A.,  
734        Turner, S., Watson, A.J., 2007. Mesoscale Iron Enrichment Experiments 1993-2005:  
735        Synthesis and Future Directions. *Science* 315, 612–617. doi:10.1126/science.1131669
- 736    Boyd, P.W., Trull, T.W., 2007. Understanding the export of biogenic particles in oceanic waters:  
737        Is there consensus? *Prog. Oceanogr.* 72, 276–312.  
738        doi:http://dx.doi.org/10.1016/j.pocean.2006.10.007
- 739    Bruland, K.W., Silver, M.W., 1981. Sinking rates of fecal pellets from gelatinous zooplankton  
740        (Salps, Pteropods, Doliolids). *Mar. Biol.* 63, 295–300. doi:10.1007/BF00395999
- 741    Buesseler, K., Ball, L., Andrews, J., Benitez-Nelson, C., Belostock, R., Chai, F., Chao, Y., 1998.  
742        Upper ocean export of particulate organic carbon in the Arabian Sea derived from thorium-  
743        234. *Deep Sea Res. Part II* 45, 2461–2487.
- 744    Buesseler, K.O., 1998. The decoupling of production and particulate export in the surface ocean.  
745        *Global Biogeochem. Cycles* 12, 297–310.
- 746    Buesseler, K.O., 1991. Do upper-ocean sediment traps provide an accurate record of particle flux?  
747        *Nature* 353, 420–423.
- 748    Buesseler, K.O., Antia, A.N., Chen, M., Fowler, S.W., Gardner, W.D., Gustafsson, O., Harada, K.,  
749        Michaels, A.F., Rutgers van der Loeff, M., Sarin, M., 2007. An assessment of the use of  
750        sediment traps for estimating upper ocean particle fluxes. *J. Mar. Res.* 65, 345–416.
- 751    Buesseler, K.O., Ball, L., Andrews, J., Cochran, J.K., Hirschberg, D.J., Bacon, M.P., Flier, A.,  
752        Brzezinski, M., 2001. Upper ocean export of particulate organic carbon and biogenic silica in  
753        the Southern Ocean along 170°W. *Deep Sea Res. Part II* 48, 4275–4297.
- 754    Buesseler, K.O., Barber, R.T., Dickson, M.-L., Hiscock, M.R., Moore, J.K., Sambrotto, R., 2003.

755 The effect of marginal ice-edge dynamics on production and export in the Southern Ocean  
756 along 170°W. *Deep Sea Res. Part II* 50, 579–603. doi:[http://dx.doi.org/10.1016/S0967-](http://dx.doi.org/10.1016/S0967-0645(02)00585-4)  
757 0645(02)00585-4

758 Buesseler, K.O., Benitez-Nelson, C.R., Moran, S.B., Burd, A., Charette, M., Cochran, J.K.,  
759 Coppola, L., Fisher, N.S., Fowler, S.W., Gardner, W.D., 2006. An assessment of particulate  
760 organic carbon to thorium-234 ratios in the ocean and their impact on the application of  $^{234}\text{Th}$   
761 as a POC flux proxy. *Mar. Chem.* 100, 213–233.

762 Cavan, E.L., Le Moigne, F.A.C., Poulton, A.J., Tarling, G.A., Ward, P., Daniels, C.J., Frago, G.,  
763 Sanders, R.J., 2015. Attenuation of particulate organic carbon flux in the Scotia Sea,  
764 Southern Ocean, is controlled by zooplankton fecal pellets. *Geophys. Res. Lett.* 42, 821–830.  
765 doi:[10.1002/2014GL062744](https://doi.org/10.1002/2014GL062744)

766 Cedhagen, T., Cheah, W., Bracher, A., Lejzerowicz, F., 2014. Algal pigments in Southern Ocean  
767 abyssal foraminifera indicate pelagobenthic coupling. *Deep Sea Res. Part II* 108, 27–32.  
768 doi:<http://dx.doi.org/10.1016/j.dsr2.2014.07.017>

769 Cheah, W., Soppa Altenburg, M., Wiegmann, S., Laglera, L.M., Santos-Echeandia, J., Strass, V.,  
770 Ossebaer, S., Hoppema, M., Klass, C., Wolf-Gladrow, D., Bracher, A. Community structure  
771 and physiological state of phytoplankton across major oceanic fronts in the Southern Ocean.  
772 *Deep Sea Res. Part II* this issue.

773 Chen, J.H., Lawrence Edwards, R., Wasserburg, G.J., 1986.  $^{238}\text{U}$ ,  $^{234}\text{U}$  and  $^{232}\text{Th}$  in seawater.  
774 *Earth Planet. Sci. Lett.* 80, 241–251.

775 Chever, F., Bucciarelli, E., Sarthou, G., Speich, S., Arhan, M., Penven, P., Tagliabue, A., 2010.  
776 Physical speciation of iron in the Atlantic sector of the Southern Ocean along a transect from the  
777 subtropical domain to the Weddell Sea Gyre. *J. Geophys. Res. Ocean.* 115, C10059,  
778 doi:[10.1029/2009JC005880](https://doi.org/10.1029/2009JC005880)

779 Coale, K.H., Bruland, K.W., 1985.  $^{234}\text{Th}$ : $^{238}\text{U}$  disequilibria within the California Current. *Limnol.*  
780 *Oceanogr.* 30, 22–33.

781 Coale, K.H., Johnson, K.S., Chavez, F.P., Buesseler, K.O., Barber, R.T., Brzezinski, M.A.,  
782 Cochlan, W.P., Millero, F.J., Falkowski, P.G., Bauer, J.E., Wanninkhof, R.H., Kudela, R.M.,  
783 Altabet, M.A., Hales, B.E., Takahashi, T., Landry, M.R., Bidigare, R.R., Wang, X., Chase,  
784 Z., Strutton, P.G., Friederich, G.E., Gorbunov, M.Y., Lance, V.P., Hiltling, A.K., Hiscock,  
785 M.R., Demarest, M., Hiscock, W.T., Sullivan, K.F., Tanner, S.J., Gordon, R.M., Hunter,  
786 C.N., Elrod, V.A., Fitzwater, S.E., Jones, J.L., Tozzi, S., Kobal, M., Roberts, A.E.,  
787 Herndon, J., Brewster, J., Ladizinsky, N., Smith, G., Cooper, D., Timothy, D., Brown, S.L.,  
788 Selph, K.E., Sheridan, C.C., Twining, B.S., Johnson, Z.I., 2004. Southern Ocean Iron  
789 Enrichment Experiment: Carbon Cycling in High- and Low-Si Waters. *Science* 304, 408–  
790 414. doi:[10.1126/science.1089778](https://doi.org/10.1126/science.1089778)

791 Cochran, J.K., Buesseler, K.O., Bacon, M.P., Wang, H.W., Hirschberg, D.J., Ball, L., Andrews, J.,  
792 Crossin, G., Fleer, A., 2000. Short-lived thorium isotopes ( $^{234}\text{Th}$ ,  $^{228}\text{Th}$ ) as indicators of POC  
793 export and particle cycling in the Ross Sea, Southern Ocean. *Deep Sea Res. Part II* 47, 3451–  
794 3490.

795 de Jong, J., Schoemann, V., Lannuzel, D., Croot, P., de Baar, H., Tison, J.-L., 2012. Natural iron  
796 fertilization of the Atlantic sector of the Southern Ocean by continental shelf sources of the  
797 Antarctic Peninsula. *J. Geophys. Res.* 117, G01029. doi:[10.1029/2011JG001679](https://doi.org/10.1029/2011JG001679)

798 Deacon, G.E.R., 1945. Water circulation and surface boundaries in the oceans. *Q. J. R. Meteorol.*  
799 *Soc.* 71, 11–25.

800 Durkin, C.A., Estapa, M.L., Buesseler, K.O., 2015. Observations of carbon export by small  
801 sinking particles in the upper mesopelagic. *Mar. Chem.* 175, 72–81.



802 doi:10.1016/j.marchem.2015.02.011

803 Ebersbach, F., Trull, T.W., 2008. Sinking particle properties from polyacrylamide gels during the  
804 Kerguelen Ocean and Plateau compared Study (KEOPS): zooplankton control of carbon  
805 export in an area of persistent natural iron inputs in the Southern Ocean. *Limnol. Oceanogr.*  
806 53, 212–224.

807 Ebersbach, F., Trull, T.W., Davies, D.M., Bray, S.G., 2011. Controls on mesopelagic particle  
808 fluxes in the Sub-Antarctic and Polar Frontal Zones in the Southern Ocean south of Australia  
809 in summer—Perspectives from free-drifting sediment traps. *Deep Sea Res. Part II* 58, 2260–  
810 2276. doi:http://dx.doi.org/10.1016/j.dsr2.2011.05.025

811 Falkowski, P.G., Barber, R.T., Smetacek, V., 1998. Biogeochemical controls and feedbacks on  
812 ocean primary production. *Science* 281, 200–206, doi: 10.1126/science.281.5374.200

813 Francois, R., Honjo, S., Krishfield, R., Manganini, S., 2002. Factors controlling the flux of organic  
814 carbon to the bathypelagic zone of the ocean. *Global Biogeochem. Cycles* 16 (4), 1087.  
815 doi:10.1029/2001GB001722

816 Friedrich, J., Rutgers van der Loeff, M., 2002. A two-tracer ( $^{210}\text{Po}$ - $^{234}\text{Th}$ ) approach to distinguish  
817 organic carbon and biogenic silica export flux in the Antarctic Circumpolar Current. *Deep*  
818 *Sea Res. Part I* 49, 101–120.

819 Gardner, W.D., 2000. Sediment trap sampling in surface waters. Cambridge University Press,  
820 Cambridge.

821 Geibert, W., Rutgers van der Loeff, M.M., Usbeck, R., Gersonde, R., Kuhn, G., Seeberg-  
822 Elverfeldt, J., 2005. Quantifying the opal belt in the Atlantic and southeast Pacific sector of  
823 the Southern Ocean by means of  $^{230}\text{Th}$  normalization. *Global Biogeochem. Cycles* 19,  
824 GB4001. doi:10.1029/2005GB002465

825 Gordon, H.R., Wang, M., 1994. Retrieval of water-leaving radiance and aerosol optical thickness  
826 over the oceans with SeaWiFS: a preliminary algorithm. *Appl. Opt.* 33, 443–452.  
827 doi:10.1364/AO.33.000443

828 Grasshoff, K., Ehrhardt, M., Kremling, K., 1983. Methods of Seawater Analysis, 2nd ed. Verlag  
829 Chemie GmbH, Weinheim.

830 Gruber, N., Gloor, M., Fletcher, S.E.M., Doney, S.C., Dutkiewicz, S., Follows, M.J., Gerber, M.,  
831 Jacobson, A.R., Joos, F., Lindsay, K., 2009. Oceanic sources, sinks, and transport of atmospheric  
832  $\text{CO}_2$ . *Global Biogeochem. Cycles* 23, GB1005. doi: 10.1029/2008GB003349

833 Heath, R.A., 1976. Models of the diffusive–advective balance at the subtropical convergence.  
834 *Deep Sea Res. Oceanogr. Abstr.* 23, 1153–1164. doi:http://dx.doi.org/10.1016/0011-  
835 7471(76)90891-3

836 Honjo, S., Manganini, S.J., Krishfield, R.A., Francois, R., 2008. Particulate organic carbon fluxes  
837 to the ocean interior and factors controlling the biological pump: A synthesis of global  
838 sediment trap programs since 1983. *Prog. Oceanogr.* 76, 217–285.

839 Hoppe, C.J.M., Klaas, C., Ossebaar, S., Soppa, M.A., Cheah, W., Laglera, L.M., Santos-  
840 Echeandia, J., Rost, B., Wolf-Gladrow, D.A., Bracher, A., Hoppema, M., Strass, V.,  
841 Trimborn, S., this issue. Controls of primary production in two phytoplankton blooms in the  
842 Antarctic Circumpolar Current. *Deep Sea Res. Part II* . doi: 10.1016/j.dsr2.2015.10.005

843 Hoppema, M., de Baar, H.J.W., Bellerby, R.G.J., Fahrbach, E., Bakker, K., 2002. Annual export  
844 production in the interior Weddell Gyre estimated from a chemical mass balance of nutrients.  
845 *Deep Sea Res. Part II* 49, 1675–1689.

846 Hoppema, M., Fahrbach, E., de Baar, H.J.W., 2000. Surface layer balance of the southern  
847 Antarctic Circumpolar Current (prime meridian) used to derive carbon and silicate

848 consumptions and annual air-sea exchange for CO<sub>2</sub> and oxygen. *J. Geophys. Res. Ocean.*  
849 105, 11359–11371.

850 Hunt, B.P. V, Hosie, G.W., 2005. Zonal structure of zooplankton communities in the Southern  
851 Ocean South of Australia: results from a 2150 km continuous plankton recorder transect.  
852 *Deep Sea Res. Part I* 52, 1241–1271. doi:<http://dx.doi.org/10.1016/j.dsr.2004.11.019>

853 IOCCG, 2010. Atmospheric Correction for Remotely-Sensed Ocean-Colour Products. Wang M.  
854 (ed.), Reports of the International Ocean-Colour Coordinating Group, No 10. IOCCG,  
855 Dartmouth, Canada.

856 Iversen, M.H., Pakhomov, E.A., Hunt, B.P. V, Jagt, H. v, Wolf-Gladrow, D., Klaas, C., this issue.  
857 Sinkers or floaters? Contribution from salp pellets to the export flux during a large bloom  
858 event in the Southern Ocean. *Deep Sea Res. Part II*

859 Jacquet, S.H.M., Lam, P.J., Trull, T.W., Dehairs, F., 2011. Carbon export production in the  
860 subantarctic zone and polar front zone south of Tasmania. *Deep Sea Res. Part II* 58, 2277–  
861 2292. doi:[10.1016/j.dsr.2011.05.035](http://dx.doi.org/10.1016/j.dsr.2011.05.035)

862 Klaas, C., Archer, D.E., 2002. Association of sinking organic matter with various types of  
863 mineral ballast in the deep sea: Implications for the rain ratio. *Glob. Biogeochem. Cycles* 16  
864 (4), 1116. doi:[10.1029/2001GB001765](http://dx.doi.org/10.1029/2001GB001765)

865 Klunder, M.B., Laan, P., Middag, R., De Baar, H.J.W., van Ooijen, J.C., 2011. Dissolved iron in  
866 the Southern Ocean (Atlantic sector). *Deep Sea Res. Part II* 58, 2678–2694.  
867 doi:[10.1016/j.dsr.2010.10.042](http://dx.doi.org/10.1016/j.dsr.2010.10.042)

868 Knap, A.H., Michaels, A., Close, A.R., Ducklow, H., Dickson, A.G., 1996. Protocols for the joint  
869 global ocean flux study (JGOFS) core measurements. JGOFS, Repr. IOC Manuals Guid. No.  
870 29, UNESCO 1994 19, 1–210.

871 Köhler, P., Fischer, H., Munhoven, G., Zeebe, R.E., 2005. Quantitative interpretation of  
872 atmospheric carbon records over the last glacial termination. *Global Biogeochem. Cycles* 19,  
873 GB4020. doi:[10.1029/2004GB002345](http://dx.doi.org/10.1029/2004GB002345)

874 Korb, R.E., Whitehouse, M.J., Ward, P., Gordon, M., Venables, H.J., Poulton, A.J., 2012.  
875 Regional and seasonal differences in microplankton biomass, productivity, and structure  
876 across the Scotia Sea: Implications for the export of biogenic carbon. *Deep Sea Res. Part II*  
877 59–60, 67–77. doi:<http://dx.doi.org/10.1016/j.dsr.2011.06.006>

878 Laglera, L.M., Santos-Echeandía, J., Caprara, S., Monticelli, D., 2013. Quantification of iron in  
879 seawater at the low picomolar range based on optimization of bromate-ammonia-  
880 dihydroxynaphtalene system by catalytic adsorptive cathodic stripping voltammetry. *Anal.*  
881 *Chem.* 85, 2486–92. doi:[10.1021/ac303621q](http://dx.doi.org/10.1021/ac303621q)

882 Lam, P.J., Bishop, J.K.B., 2007. High biomass, low export regimes in the Southern Ocean. *Deep*  
883 *Sea Res. Part II* 54, 601–638. doi:<http://dx.doi.org/10.1016/j.dsr.2007.01.013>

884 Landschützer, P., Gruber, N., Haumann, F.A., Rödenbeck, C., Bakker, D.C.E., van Heuven, S.,  
885 Hoppema, M., Metzl, N., Sweeney, C., Takahashi, T., Tilbrook, B., Wanninkhof, R., 2015.  
886 The reinvigoration of the Southern Ocean carbon sink. *Science* 349, 1221–1224. doi:  
887 [10.1126/science.aab2620](http://dx.doi.org/10.1126/science.aab2620)

888 Laubscher, R.K., Perissinotto, R., McQuaid, C.D., 1993. Phytoplankton production and biomass at  
889 frontal zones in the Atlantic sector of the Southern Ocean. *Polar Biol.* 13, 471–481.

890 Laurenceau-Cornec, E.C., Trull, T.W., Davies, D.M., Bray, S.G., Doran, J., Planchon, F., Carlotti,  
891 F., Jouandet, M.-P., Cavagna, A.-J., Waite, A.M., Blain, S., 2015. The relative importance of  
892 phytoplankton aggregates and zooplankton fecal pellets to carbon export: insights from free-  
893 drifting sediment trap deployments in naturally iron-fertilised waters near the Kerguelen  
894 Plateau. *Biogeosciences* 12, 1007–1027. doi:[10.5194/bg-12-1007-2015](http://dx.doi.org/10.5194/bg-12-1007-2015)

895 Le Moigne, F.A.C., Boye, M., Masson, A., Corvaisier, R., Grossteffan, E., Guéneugues, A.,  
896 Pondaven, P., 2013a. Description of the biogeochemical features of the subtropical  
897 southeastern Atlantic and the Southern Ocean south of South Africa during the austral  
898 summer of the International Polar Year. *Biogeosciences* 10, 281–295. doi:10.5194/bg-10-281-  
899 2013

900 Le Moigne, F.A.C., Henson, S.A., Sanders, R.J., Madsen, E., 2013b. Global database of surface  
901 ocean particulate organic carbon export fluxes diagnosed from the  $^{234}\text{Th}$  technique. *Earth*  
902 *Syst. Sci. Data* 5, 295–304. doi:10.5194/essd-5-295-2013

903 Madin, L.P., 1982. Production, composition and sedimentation of salp fecal pellets in oceanic  
904 waters. *Mar. Biol.* 67, 39–45.

905 Maiti, K., Buesseler, K.O., Pike, S.M., Benitez-Nelson, C., Cai, P., Chen, W., Cochran, K., Dai,  
906 M., Dehairs, F., Gasser, B., Kelly, R.P., Masqué, P., Miller, L.A., Miquel, J.C., Moran, S.B.,  
907 Morris, P.J., Peine, F., Planchon, F., Renfro, A.A., Rutgers van der Loeff, M., Santschi, P.H.,  
908 Turnewitsch, R., Waples, J.T., Xu, C., 2012. Intercalibration studies of short-lived Thorium-  
909 234 in the water column and marine particles. *Limnol. Ocean. Methods* 10, 631–644.  
910 doi:10.4319/lom.2012.10.631

911 Maiti, K., Charette, M.A., Buesseler, K.O., Kahru, M., 2013. An inverse relationship between  
912 production and export efficiency in the Southern Ocean. *Geophys. Res. Lett.* 40, 1557–1561.  
913 doi:doi:10.1002/grl.50219

914 Manno, C., Stowasser, G., Enderlein, P., Fielding, S., Tarling, G.A., 2015. The contribution of  
915 zooplankton faecal pellets to deep-carbon transport in the Scotia Sea (Southern Ocean).  
916 *Biogeosciences* 12, 1955–1965. doi:10.5194/bg-12-1955-2015

917 Millero, F.J., Sotolongo, S., Izaguirre, M., 1987. The kinetics of oxidation of Fe(II) in seawater.  
918 *Geochim. Cosmochim. Acta* 51, 793–801. doi:10.1016/0016-7037(87)90093-7

919 Mizdalski, E., 1988. Weight and length data of zooplankton in the Weddell Sea in austral spring  
920 1986 (ANT V/3). *Berichte zur Polarforsch. Reports Polar Res.* 55. Bremerhaven, Germany

921 Moore, R.M., Millward, G.E., 1988. The kinetics of reversible Th reactions with marine particles.  
922 *Geochim. Cosmochim. Acta* 52, 113–118.

923 Morel, A., Maritorena, S., 2001. Bio-optical properties of oceanic waters: A reappraisal. *J.*  
924 *Geophys. Res. Ocean.* 106, 7163–7180. doi:10.1029/2000JC000319

925 Murphy, J., Riley, J.P., 1962. A modified single solution method for the determination of  
926 phosphate in natural waters. *Anal. Chim. Acta* 27, 31–36. doi: 10.1016/S0003-  
927 2670(00)88444-5

928 Nowlin, W.D., Klinck, J.M., 1986. The physics of the Antarctic circumpolar current. *Rev.*  
929 *Geophys.* 24, 469–491.

930 OC-CCI, 2015. Ocean Color Climate Change Initiative Product User Guide Version 2. Plymouth  
931 Marine Laboratory, Plymouth, UK.

932 Orsi, A.H., Whitworth, T., Nowlin, W.D., 1995. On the meridional extent and fronts of the  
933 Antarctic Circumpolar Current. *Deep Sea Res. Part I* 42, 641–673.

934 Owens, S.A., Buesseler, K.O., Sims, K.W.W., 2011. Re-evaluating the  $^{238}\text{U}$ -salinity relationship  
935 in seawater: Implications for the  $^{238}\text{U}$ - $^{234}\text{Th}$  disequilibrium method. *Mar. Chem.* 127, 31–39.

936 Owens, S.A., Pike, S., Buesseler, K.O., 2015. Thorium-234 as a tracer of particle dynamics and  
937 upper ocean export in the Atlantic Ocean. *Deep Sea Res. Part II* 116, 42–59.  
938 doi:http://dx.doi.org/10.1016/j.dsr2.2014.11.010

939 Pakhomov, E.A., McQuaid, C.D., 1996. Distribution of surface zooplankton and seabirds across  
940 the Southern Ocean. *Polar Biol.* 16, 271–286.

- 941 Perissinotto, R., Pakhomov, E.A., 1998. Contribution of salps to carbon flux of marginal ice zone  
942 of the Lazarev Sea, Southern Ocean. *Mar. Biol.* 131, 25–32.
- 943 Phillips, B., Kremer, P., Madin, L.P., 2009. Defecation by *Salpa thompsoni* and its contribution to  
944 vertical flux in the Southern Ocean. *Mar. Biol.* 156, 455–467.
- 945 Pike, S.M., Buesseler, K.O., Andrews, J., Savoye, N., 2005. Quantification of Th-234 recovery in  
946 small volume seawater samples by inductively coupled plasma-mass spectrometry. *J.*  
947 *Radioanal. Nucl. Chem.* 263, 355–360.
- 948 Planchon, F., Ballas, D., Cavagna, A.-J., Bowie, A.R., Davies, D., Trull, T., Laurenceau-Cornec,  
949 E.C., Van Der Merwe, P., Dehairs, F., 2015. Carbon export in the naturally iron-fertilized  
950 Kerguelen area of the Southern Ocean based on the <sup>234</sup>Th approach. *Biogeosciences* 12,  
951 3831–3848. doi:10.5194/bg-12-3831-2015
- 952 Planchon, F., Cavagna, A.-J., Cardinal, D., André, L., Dehairs, F., 2013. Late summer particulate  
953 organic carbon export and twilight zone remineralisation in the Atlantic sector of the  
954 Southern Ocean. *Biogeosciences* 10, 803–820. doi:10.5194/bg-10-803-2013
- 955 Pollard, R.T., Bathmann, U., Dubischar, C., Read, J.F., Lucas, M., 2002a. Zooplankton  
956 distribution and behaviour in the Southern Ocean from surveys with a towed Optical  
957 Plankton Counter. *Deep Sea Res. Part II* 49, 3889–3915. doi: 10.1016/S0967-  
958 0645(02)00116-9
- 959 Pollard, R.T., Lucas, M.I., Read, J.F., 2002b. Physical controls on biogeochemical zonation in the  
960 Southern Ocean. *Deep Sea Res. Part II* 49, 3289–3305. doi: 10.1016/S0967-0645(02)00084-  
961 X
- 962 Puigcorbé, V., Benitez-Nelson, C.R., Masqué, P., Verdeny, E., White, A.E., Popp, B.N., Prahl,  
963 F.G., Lam, P.J., 2015. Small phytoplankton drive high summertime carbon and nutrient  
964 export in the Gulf of California and Eastern Tropical North Pacific. *Global Biogeochem.*  
965 *Cycles* 29, 1309–1332. doi:10.1002/ 2015GB005134
- 966 Quéguiner, B., 2013. Iron fertilization and the structure of planktonic communities in high nutrient  
967 regions of the Southern Ocean. *Deep. Res. Part II* 90, 43–54. doi:10.1016/j.dsr2.2012.07.024
- 968 Read, J.F., Pollard, R.T., Bathmann, U., 2002. Physical and biological patchiness of an upper  
969 ocean transect from South Africa to the ice edge near the Greenwich Meridian. *Deep Sea*  
970 *Res. Part II* 49, 3713–3733.
- 971 Rembauville, M., Blain, S., Armand, L., Quéguiner, B., Salter, I., 2015a. Export fluxes in a  
972 naturally iron-fertilized area of the Southern Ocean – Part 2: Importance of diatom resting  
973 spores and faecal pellets for export. *Biogeosciences* 12, 3171–3195. doi:10.5194/bg-12-3171-  
974 2015
- 975 Rembauville, M., Salter, I., Leblond, N., Gueneugues, A., Blain, S., 2015b. Export fluxes in a  
976 naturally iron-fertilized area of the Southern Ocean – Part 1: Seasonal dynamics of particulate  
977 organic carbon export from a moored sediment trap. *Biogeosciences* 12, 3153–3170.  
978 doi:10.5194/bg-12-3153-2015
- 979 Resplandy, L., Martin, A.P., Le Moigne, F., Martin, P., Aquilina, A., Mémery, L., Lévy, M.,  
980 Sanders, R., 2012. How does dynamical spatial variability impact <sup>234</sup>Th-derived estimates of  
981 organic export? *Deep Sea Res. Part I* 68, 24–45.  
982 doi:http://dx.doi.org/10.1016/j.dsr.2012.05.015
- 983 Roca-Martí, M., Puigcorbé, V., Iversen, M.H., Rutgers van der Loeff, M., Klaas, C., Cheah, W.,  
984 Bracher, A., Masqué, P., this issue. Particulate organic carbon export during the decline of a  
985 vast diatom bloom in the Atlantic sector of the Southern Ocean. *Deep Sea Res. Part II.*  
986 doi:10.1016/j.dsr2.2015.12.007
- 987 Rosengard, S.Z., Lam, P.J., Balch, W.M., Auro, M.E., Pike, S., Drapeau, D., Bowler, B., 2015.

988 Carbon export and transfer to depth across the Southern Ocean Great Calcite Belt.  
989 Biogeosciences 12, 3953–3971. doi:10.5194/bg-12-3953-2015

990 Ruff, S.E., Probandt, D., Zinkann, A.-C., Iversen, M.H., Klaas, C., Würzberg, L., Krombholz, N.,  
991 Wolf-Gladrow, D., Amann, R., Knittel, K., 2014. Indications for algae-degrading benthic  
992 microbial communities in deep-sea sediments along the Antarctic Polar Front. Deep Sea Res.  
993 Part II 108, 6–16. doi:http://dx.doi.org/10.1016/j.dsr2.2014.05.011

994 Rutgers van der Loeff, M., Cai, P., Stimac, I., Bracher, A., Middag, R., Klunder, M., van Heuven,  
995 S., 2011. <sup>234</sup>Th in surface waters: distribution of particle export flux across the Antarctic  
996 Circumpolar Current and in the Weddell Sea during the GEOTRACES expedition ZERO and  
997 DRAKE. Deep Sea Res. Part II 58, 2749–2766. doi:10.1016/j.dsr2.2011.02.004

998 Rutgers van der Loeff, M.M., Buesseler, K., Bathmann, U., Hense, I., Andrews, J., 2002.  
999 Comparison of carbon and opal export rates between summer and spring bloom periods in the  
000 region of the Antarctic Polar Front, SE Atlantic. Deep Sea Res. Part II 49, 3849–3869.

001 Rutgers van der Loeff, M.M., Friedrich, J., Bathmann, U. V, 1997. Carbon export during the  
002 spring bloom at the Antarctic Polar Front, determined with the natural tracer <sup>234</sup>Th. Deep Sea  
003 Res. Part II 44, 457–478.

004 Salter, I., Kemp, A.E.S., Moore, C.M., Lampitt, R.S., Wolff, G.A., Holtvoeth, J., 2012. Diatom  
005 resting spore ecology drives enhanced carbon export from a naturally iron-fertilized bloom in  
006 the Southern Ocean. Global Biogeochem. Cycles 26, GB1014. doi:10.1029/2010GB003977

007 Santschi, P.H., Murray, J.W., Baskaran, M., Benitez-Nelson, C.R., Guo, L.D., Hung, C.C.,  
008 Lamborg, C., Moran, S.B., Passow, U., Roy-Barman, M., 2006. Thorium speciation in  
009 seawater. Mar. Chem. 100, 250–268.

010 Sarmiento, J.L., Gruber, N., Brzezinski, M.A., Dunne, J.P., 2004. High-latitude controls of  
011 thermocline nutrients and low latitude biological productivity. Nature 427, 56–60.

012 Savoye, N., Benitez-Nelson, C., Burd, A.B., Cochran, J.K., Charette, M., Buesseler, K.O.,  
013 Jackson, G.A., Roy-Barman, M., Schmidt, S., Elskens, M., 2006. <sup>234</sup>Th sorption and export  
014 models in the water column: a review. Mar. Chem. 100, 234–249.  
015 doi:10.1016/j.marchem.2005.10.014

016 Savoye, N., Trull, T.W., Jacquet, S.H.M., Navez, J., Dehairs, F., 2008. <sup>234</sup>Th-based export fluxes  
017 during a natural iron fertilization experiment in the Southern Ocean (KEOPS). Deep Sea  
018 Res. Part II 55, 841–855. doi:10.1016/j.dsr2.2007.12.036

019 Schlitzer, R., 2002. Carbon export fluxes in the Southern Ocean: Results from inverse modeling  
020 and comparison with satellite-based estimates. Deep Sea Res. Part II 49, 1623–1644.

021 Smetacek, V., Klaas, C., Strass, V.H., Assmy, P., Montresor, M., Cisewski, B., Savoye, N., Webb,  
022 A., d'Ovidio, F., Arrieta, J.M., others, 2012. Deep carbon export from a Southern Ocean  
023 iron-fertilized diatom bloom. Nature 487, 313–319. doi:10.1038/nature11229

024 Smith, K.L., Ruhl, H.A., Kahru, M., Huffard, C.L., Sherman, A.D., 2013. Deep ocean  
025 communities impacted by changing climate over 24 y in the abyssal northeast Pacific Ocean.  
026 Proc. Natl. Acad. Sci. 110, 19838–19841. doi:10.1073/pnas.1315447110

027 Smythe-Wright, D., Chapman, P., Rae, C.D., Shannon, L. V, Boswell, S.M., 1998. Characteristics  
028 of the South Atlantic subtropical frontal zone between 15°W and 5°E. Deep Sea Res. Part I  
029 45, 167–192. doi:http://dx.doi.org/10.1016/S0967-0637(97)00068-X

030 Sokolov, S., Rintoul, S.R., 2007. On the relationship between fronts of the Antarctic Circumpolar  
031 Current and surface chlorophyll concentrations in the Southern Ocean. J. Geophys. Res.  
032 Ocean. 112, C07030. doi:10.1029/2006JC004072

- 033 Steinmetz, F., Deschamps, P.-Y., Ramon, D., 2011. Atmospheric correction in presence of sun  
034 glint: application to MERIS. *Opt. Express* 19, 9783–9800. doi:10.1364/OE.19.009783
- 035 Strass, V.H., Garabato, A.C.N., Bracher, A.U., Pollard, R.T., Lucas, M.I., 2002a. A 3-D  
036 mesoscale map of primary production at the Antarctic Polar Front: results of a diagnostic  
037 model. *Deep Sea Res. Part II* 49, 3813–3834. doi:http://dx.doi.org/10.1016/S0967-  
038 0645(02)00112-1
- 039 Strass, V.H., Leach, H., Prandke, H., Donnelly, M., Bracher, A.U., Wolf-Gladrow, D.A., n.d. The  
040 physical environmental conditions for biogeochemical differences along the Antarctic  
041 Circumpolar Current in the Atlantic Sector during late austral summer 2012. *Deep Sea Res.*  
042 *Part II*, this issue
- 043 Strass, V.H., Naveira Garabato, A.C., Pollard, R.T., Fischer, H.I., Hense, I., Allen, J.T., Read, J.F.,  
044 Leach, H., Smetacek, V., 2002b. Mesoscale frontal dynamics: shaping the environment of  
045 primary production in the Antarctic Circumpolar Current. *Deep Sea Res. Part II* 49, 3735–  
046 3769.
- 047 Strickland, J.D.H., Parsons, T.R., 1968. A practical handbook of seawater analysis. *Bull. Fish.*  
048 *Res. Board Canada* 167, 1-310.
- 049 Takahashi, T., Sutherland, S.C., Wanninkhof, R., Sweeney, C., Feely, R.A., Chipman, D.W.,  
050 Hales, B., Friederich, G., Chavez, F., Sabine, C., Watson, A., Bakker, D.C.E., Schuster, U.,  
051 Metzl, N., Yoshikawa-Inoue, H., Ishii, M., Midorikawa, T., Nojiri, Y., Körtzinger, A.,  
052 Steinhoff, T., Hoppema, M., Olafsson, J., Arnarson, T.S., Tilbrook, B., Johannessen, T.,  
053 Olsen, A., Bellerby, R., Wong, C.S., Delille, B., Bates, N.R., de Baar, H.J.W., 2009.  
054 Climatological mean and decadal change in surface ocean pCO<sub>2</sub>, and net sea–air CO<sub>2</sub> flux  
055 over the global oceans. *Deep Sea Res. Part II* 56, 554–577. doi:DOI:  
056 10.1016/j.dsr2.2008.12.009
- 057 Tomczak, M., Godfrey, J.S., 2001. *Regional oceanography: an introduction*. Pergamon, Oxford.
- 058 Tréguer, P.J., De La Rocha, C.L., 2013. The world ocean silica cycle. *Ann. Rev. Mar. Sci.* 5, 477–  
059 501. doi: 10.1146/annurev-marine-121211-172346
- 060 Turner, J.T., 2002. Zooplankton fecal pellets, marine snow and sinking phytoplankton blooms.  
061 *Aquat. Microb. Ecol.* 27, 57–102.
- 062 Uitz, J., Claustre, H., Griffiths, F.B., Ras, J., Garcia, N., Sandroni, V., 2009. A phytoplankton  
063 class-specific primary production model applied to the Kerguelen Islands region (Southern  
064 Ocean). *Deep. Res. Part I* 56, 541–560. doi:10.1016/j.dsr.2008.11.006
- 065 Usbeck, R., Schlitzer, R., Fischer, G., Wefer, G., 2003. Particle fluxes in the ocean: comparison of  
066 sediment trap data with results from inverse modeling. *J. Mar. Syst.* 39, 167–183.  
067 doi:http://dx.doi.org/10.1016/S0924-7963(03)00029-0
- 068 Ward, P., 1989. The distribution of zooplankton in an Antarctic fjord at South Georgia during  
069 summer and winter. *Antarct. Sci.* 1, 141–150.
- 070 Whitworth, T., Nowlin, W.D., 1987. Water masses and currents of the Southern Ocean at the  
071 Greenwich Meridian. *J. Geophys. Res. Ocean.* 92, 6462–6476.  
072 doi:10.1029/JC092iC06p06462
- 073 Wolf-Gladrow, D., 2013. The Expedition of the Research Vessel “Polarstern” to the Antarctic in  
074 2012 (ANT-XXVIII/3). Reports on Polar and Marine Research 661. Bremerhaven, Germany.
- 075